Quaternary Science Reviews 228 (2020) 106075

Contents lists available at ScienceDirect

Quaternary Science Reviews

journal homepage: www.elsevier.com/locate/quascirev

Changes in western Mediterranean thermohaline circulation in association with a deglacial Organic Rich Layer formation in the Alboran Sea

José N. Pérez-Asensio [a, *], Jaime Frigola [a], Leopoldo D. Pena [a], Francisco J. Sierro [b], María Isabel Reguera [c], Francisco J. Rodríguez-Tovar [d], Javier Dorador [e], Alessandra Asioli [f], Jannis Kuhlmann [g], Katrin Huhn [g], Isabel Cacho [a]

[a] GRC Geociències Marines, Departament de Dinàmica de la Terra i de l'Oceà, Facultat de Ciències de la Terra, Universitat de Barcelona, Carrer Martí i Franquès s/n, 08028 Barcelona, Spain
[b] Department of Geology, University of Salamanca, 37008 Salamanca, Spain
[c] IGME - Geological Survey of Spain, 28003 Madrid, Spain
[d] Departamento de Estratigrafía y Paleontología, Universidad de Granada, Fuente Nueva s/n, 18002 Granada, Spain
[e] Department of Earth Sciences, Royal Holloway University of London, TW20 0EX Egham, United Kingdom
[f] CNR-ISMAR, Consiglio Nazionale delle Ricerche, Istituto di Scienze Marine, Sede Bologna, 40129 Bologna, Italy
[g] MARUM-Center for Marine Environmental Sciences, University of Bremen, Bremen, Germany

ARTICLE INFO

Article history:
Received 24 May 2019
Received in revised form
14 November 2019
Accepted 14 November 2019
Available online 5 December 2019

Keywords:
Micropaleontology
Foraminifers
Ichnology
Stable isotopes
Organic matter flux
Thermohaline circulation
Paleoceanography
Organic Rich Layer (ORL)
Western Mediterranean
Late glacial
Holocene

ABSTRACT

The accumulation of an Organic Rich Layer (ORL) during the last deglaciation in the Alboran Sea (western Mediterranean Sea) and its link to changes in deep and intermediate water circulation are here investigated. Benthic foraminiferal assemblages and the shallow infaunal foraminifer *Uvigerina peregrina* $\delta^{13}C$ record support the establishment of sustained high organic matter fluxes, and thus eutrophic conditions at the sea floor, during the late phase of the ORL (Younger Dryas to early Holocene periods). Since organic matter fluxes were lower (mesotrophic conditions) during the Bølling-Allerød period, they cannot be solely responsible for the ORL initiation. Geochemical, sedimentological and micropalaeontological proxies support a major weakening of the deep-water convection in the Gulf of Lion as the main driver for the development of poorly-ventilated conditions from intermediate depths (946 m) to the deep western Mediterranean basin that promoted the beginning of the ORL deposition. Nevertheless, a better ventilation at intermediate depths was established during the late ORL, while the deep basin remained poorly ventilated. We propose that our data reflect the arrival of a new better-ventilated intermediate water mass analogue to the current Levantine Intermediate Water (LIW) and/or a new intermediate water mass from the Gulf of Lion. The ultimate source of this water mass needs to be further explored but chronologies of the changes recorded here indicate that intermediate and deep ventilation phases were decoupled between the western and eastern Mediterranean basins during the deglaciation and early-middle Holocene.

1. Introduction

The most important events related to fluctuations in dissolved oxygen content and organic matter fluxes in the Alboran Sea and other western Mediterranean Sea regions are the depositions of the Organic Rich Layers (ORLs). Several ORLs, defined as dark sediment layers with organic carbon higher than 0.8%, have been recorded in the Alboran Sea during the last 3 Ma (Murat, 1999). Western Mediterranean ORLs deposition might be originated by hydrological and productivity changes related to the Atlantic inflow and wind-driven meso-scale gyres (Murat, 1999). Eastern Mediterranean sapropels are also organic rich layers, but their organic matter content is higher (>2%) (Kidd et al., 1978), and their driving mechanisms are water column stratification due to high riverine discharge, and high organic matter fluxes (Emeis et al., 2000). The deposition of the most recent Organic Rich Layer (ORL) in the

* Corresponding author.
E-mail address: perez@cerege.fr (J.N. Pérez-Asensio).

https://doi.org/10.1016/j.quascirev.2019.106075

Alboran Sea took place during the deglaciation and early Holocene (14.35–8.9 ka) (Cacho et al., 2002; Martinez-Ruiz et al., 2015). The enhanced organic matter accumulation and preservation that formed this ORL on the deep-sea floor has been attributed to a weakening in bottom water circulation in the western Mediterranean, probably caused by surface water stratification during deglacial sea level rise (Rogerson et al., 2008). Changes in bottom water oxygen content and organic matter fluxes across the most recent ORL have been investigated in deep sites from the Alboran Sea (e.g., Bárcena et al., 2001; Cacho et al., 2002; Rogerson et al., 2008; Rodrigo-Gámiz et al., 2011; Martinez-Ruiz et al., 2015). However, studies focusing on intermediate waters are still scarce (Ausín et al., 2015a, 2015b) and consequently little is known about the impact of the described ORL-related changes in circulation and organic matter fluxes at intermediate depths.

A powerful tool to unravel deep water oxygen content and organic matter fluxes to the sea floor are benthic microorganisms (foraminifera) and macrobenthic trace makers (burrowing organisms) due to their sensitivity to both variations in bottom water oxygen levels and organic matter supply (e.g., Murray, 2006; Jorissen et al., 2007; Aguirre et al., 2010; Quiroz et al., 2010; Rodríguez-Tovar and Dorador, 2014; Rodríguez-Tovar et al., 2015a, 2015b). Ichnological properties such as ichnodiversity, abundance of bioturbation, size of traces or depth of burrow penetration, are narrowly related with availability of organic matter, oxygen flux into the sediment and sedimentation rate in deep-marine settings (e.g., Uchman and Wetzel, 2011; Wetzel and Uchman, 2012). Dissolved oxygen content and organic matter supply are intimately related due to the remineralisation of organic matter, which consumes oxygen (Jorissen et al., 1995; Mojtahid et al., 2009). These trophic and oxygen conditions control benthic foraminiferal microhabitat preferences, that is their living depth within the sediment (Jorissen et al., 1995). In eutrophic environments, deep infaunal benthic foraminifera dominate. In mesotrophic environments, all microhabitats (deep infaunal to epifaunal) are well-represented. Oligotrophic environments are characterised by a dominance of epifaunal benthic foraminifera (Jorissen et al., 1995). Foraminiferal stable oxygen ($\delta^{18}O$) and carbon ($\delta^{13}C$) isotopes are also useful proxies to investigate productivity and organic matter fluxes (planktic and benthic stable $\delta^{13}C$ isotopes), bottom water ventilation (benthic stable $\delta^{13}C$ isotopes) and glacial-deglacial changes (foraminiferal stable $\delta^{18}O$ isotopes) (Rohling and Cooke, 1999; Mackensen, 2008).

The governing mechanisms for changes in oxygen content and organic matter fluxes are diverse. Firstly, deep water convection ventilates bottom waters supplying dissolved oxygen to the bottom of the basin (Murray, 2006; Pemberton et al., 2001; Jorissen et al., 2007). Secondly, fluxes of organic matter reaching the sea floor are mainly controlled by surface ocean primary productivity, upwelling events, lateral advection of organic particles, the input of terrestrial organic carbon transported to the sea by rivers, and organic matter remineralisation along the water column (Gardner et al., 1985; Bakun, 1990; Asper et al., 1992; Takahashi et al., 1993; Hedges et al., 1997; Thunell et al., 2007). The Alboran Sea, located in the westernmost Mediterranean Sea, is affected by deep and intermediate water currents, upwelling, riverine discharge, and lateral advection processes, which control bottom water dissolved oxygen and organic matter inputs to the sea floor (García-Gorriz and Carr, 1999; Millot, 1999, 2009; Sarhan et al., 2000). The main goal of this study is to disentangle changes in bottom water oxygen and organic matter fluxes at intermediate depths of the Alboran Sea in relation to western Mediterranean deep basin conditions across the most recent ORL deposition. We present results from benthic foraminifera and trace fossil assemblages (benthic micro- and macrofauna), as well as planktic and benthic foraminiferal stable oxygen ($\delta^{18}O$) and carbon ($\delta^{13}C$) isotopes and Total Organic Carbon (TOC) contents, measured at the intermediate depth (946 m) gravity core HER-GC-UB6 from the Alboran Sea (Fig. 1). This information is analysed in comparison with benthic foraminifera, benthic foraminiferal stable carbon ($\delta^{13}C$) isotopes, TOC contents, alkenones and grain size data from the nearby deep site MD95-2043 (1841 m) in the Alboran Sea, and the deep site MD99-2343 (2391 m) from the Minorca Rise (Fig. 1), which most of them form part of previous published studies (Cacho et al., 2002; Reguera, 2004; Frigola et al., 2008).

2. Study area and oceanographic setting

The Mediterranean Sea circulation forms a thermohaline system, which is driven by its negative hydrologic budget (concentration basin) due to excess of evaporation over freshwater input (river runoff + rainfall) (Béthoux, 1980). This deficit is balanced through anti-estuarine water exchange across the Strait of Gibraltar where lower salinity Atlantic surface waters flow eastward into the Mediterranean and more saline Mediterranean deep and intermediate waters enter the Atlantic as a bottom current (Mediterranean Outflow Water, MOW) (Wüst, 1961; Pinardi and Masetti, 2000; Malanotte-Rizzoli et al., 2014).

The Alboran Sea is located in the westernmost Mediterranean Sea and it is connected to the Atlantic Ocean through the Strait of Gibraltar (Fig. 1A). It is the first Mediterranean basin receiving the Atlantic Water (AW) influx, the so-called Atlantic Jet, which forms two semi-permanent anticyclonic gyres (the Western and Eastern Anticyclonic Gyres) (La Violette, 1986; Heburn and La Violette, 1990). At the northern margin of these anticyclonic gyres, there is a frontal system generating quasi-permanent areas of upwelling (García-Gorriz and Carr, 1999). The Alboran Sea basin is filled by three different water masses (Fig. 1B). The upper water layer is the Modified Atlantic Water (MAW) (0–220 m), which is formed from the AW that gradually increases its temperature and salinity while flowing eastwards (Gascard and Richez, 1985; Parrilla et al., 1986). The AW has high dissolved oxygen concentration and low nutrient concentration (García-Martínez et al., 2019). The middle water layer is the Levantine Intermediate Water (LIW) (220–600 m), a saline and warm water mass that is formed by winter convection in the eastern Mediterranean (Wüst, 1961; Marshall and Schott, 1999; Millot, 1999, 2009; Schroeder et al., 2012). The LIW is characterised by a nutrient maximum and a dissolved oxygen minimum (García-Martínez et al., 2019). The lower water layer is the Western Mediterranean Deep Water (WMDW) (>600 m), which is produced in the Gulf of Lion due to intense north-westerly winds during severe winters causing cooling and evaporation of surface waters (MEDOC Group, 1970; Bryden and Stommel, 1984; Lacombe et al., 1985). The WMDW formation also depends on the amount and depth of the LIW arriving at the Gulf of Lion prior to WMDW formation events (Pinardi and Masetti, 2000). The WMDW shows higher dissolved oxygen concentration and lower nutrient concentration than LIW (García-Martínez et al., 2019).

3. Material and methods

The studied material is the gravity core HER-GC-UB6 (36°14′23.78″N, 3°59′21.17″W) recovered at 946 m water depth in the Alboran Sea during the HERMESIONE oceanographic cruise onboard the *BIO Hespérides* vessel (October 2009) (Fig. 1). This core is 255 cm-long and it was divided into three core sections from top to bottom: HER-GC-UB06-S1 (94 cm), HER-GC-UB06-S2 (100 cm) and HER-GC-UB06-S3 (61 cm). The core is mostly composed by homogeneous greyish clays very rich in foraminifera. Additionally, data of benthic foraminifera, benthic foraminiferal stable carbon

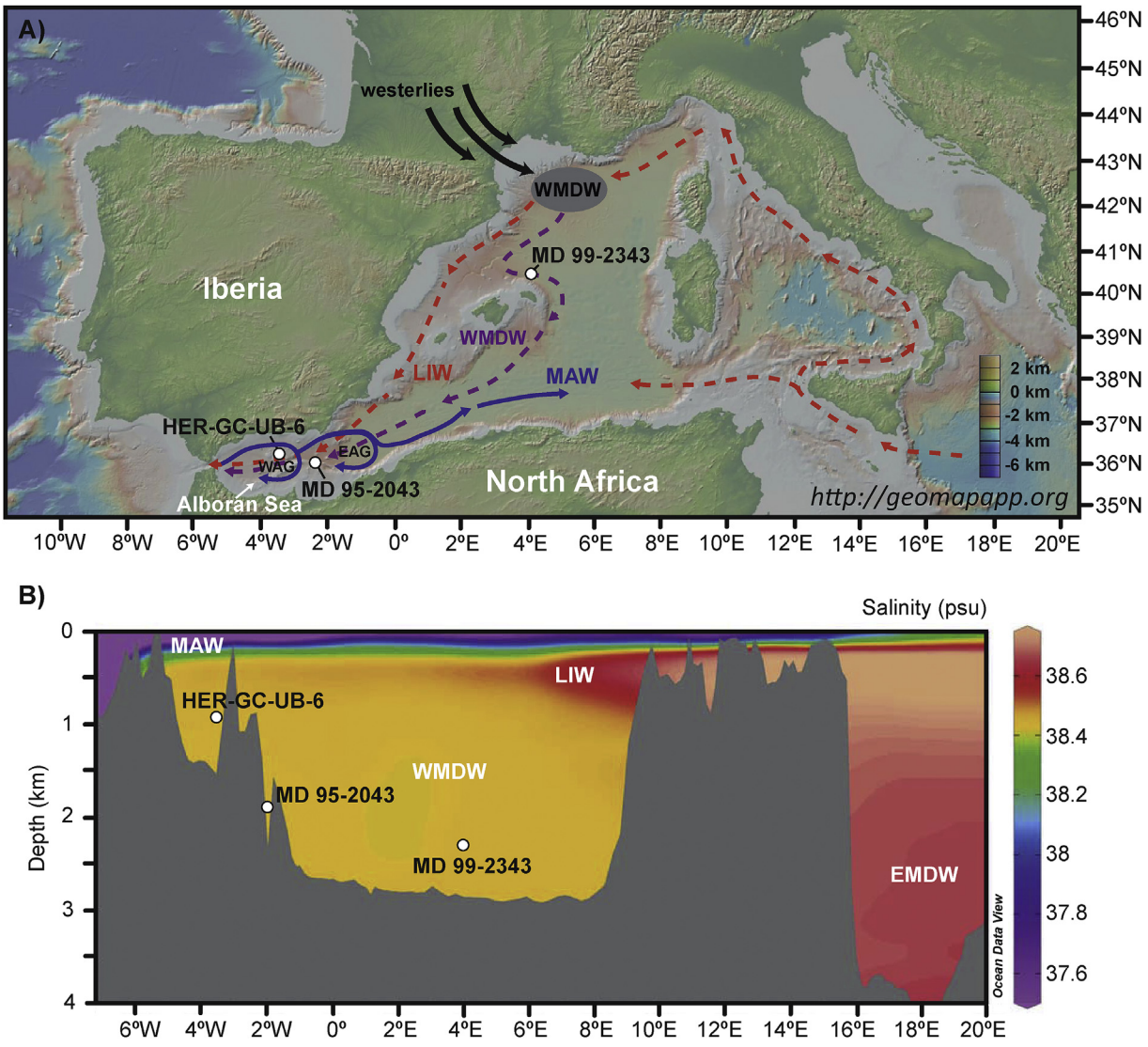

Fig. 1. Simplified modern hydrography of the western Mediterranean Sea including the Alboran Sea (Millot, 1999). (a) Location of the studied core (HER-GC-UB6) and the complementary cores (MD95-2043, MD99-2343). Surficial water masses (solid lines), intermediate and deep water masses (dashed lines) and WMDW formation area (grey ellipse) are indicated. Western Anticyclonic Gyre (WAG) and Eastern Anticyclonic Gyre (EAG) are also shown. (b) Vertical distribution of the water masses in the western Mediterranean derived from salinity data (Schlitzer, 2009). Abbreviations are: MAW, Modified Atlantic Water; LIW, Levantine Intermediate Water; WMDW, Western Mediterranean Deep Water; EMDW, Eastern Mediterranean Deep Water.

($\delta^{13}C$) isotopes and TOC contents from the piston cores MD95-2043 (western Alboran Sea, 1841 m water depth) and MD99-2343 (Minorca Rise, 2391 m water depth) (Fig. 1) were used for comparison (Cacho et al., 2002, 2006; Reguera, 2004; Frigola et al., 2008).

3.1. Age model

The age model for the core HER-GC-UB6 is based on eleven ^{14}C accelerator mass spectrometry (AMS) radiocarbon ages measured in planktic foraminifera picked from the size fraction >250 μm (Fig. 2; Table 1). Eight of the radiocarbon dates were obtained from monospecific samples of *Globoconella inflata*, two radiocarbon dates were measured on monospecific samples of *Neogloboquadrina pachyderma*, and one radiocarbon date is based on a multispecific sample of *G. inflata* and *N. pachyderma* (Table 1). The eleven radiocarbon ages were calibrated by using the regional average marine reservoir correction (ΔR) for the western Mediterranean Sea (−22.0 ± 35.0) and the Calib 7.10 software (Stuiver and Reimer, 1993) and the MARINE13 calibration curve (Reimer et al., 2013). Age uncertainties are expressed as 2σ errors (Table 1). The age model was constructed with the Bayesian statistics software Bacon v2.2 (Blaauw and Christen, 2011) with the statistical package RStudio v1.1.463. Before performing the Bayesian accumulation model, sedimentation rates derived from the eleven radiocarbon dates were calculated in order to detect abrupt changes. Since a sharp increase in sedimentation rate was recorded at 7.5 ka (135 cm core depth), it was decided to apply the Bayesian accumulation model for the upper (0–135 cm) and lower (135–255 cm) parts of the core, separately. This approached resulted in a better fit for the Bayesian accumulation model.

3.2. Benthic foraminiferal analysis

3.2.1. Core HER-GC-UB6

Forty-four freeze-dried 1-cm-thick samples (5–10 g) were

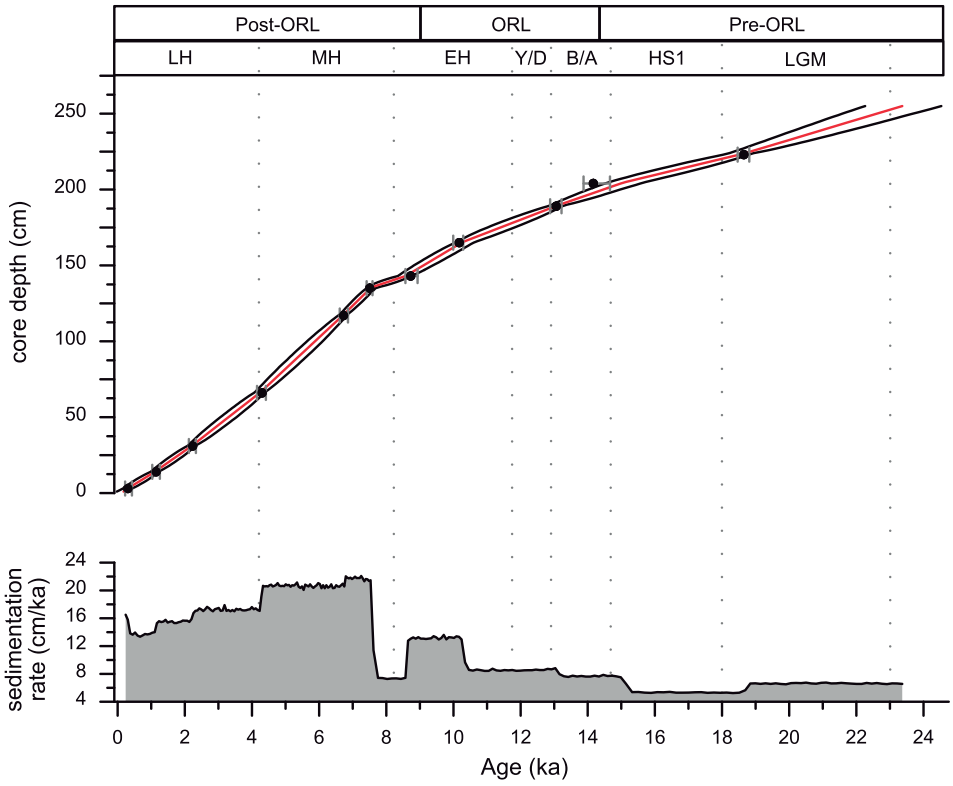

Fig. 2. Age-depth model based on Bayesian accumulation simulation (Blaauw and Christen, 2011) and sedimentation rates (cm/ka) for the core HER-GC-UB6. Calibrated ages (black dots) and their uncertainties expressed as 2σ errors (grey horizontal bars) are shown. Red line represents the calculated mean, and grey lines encompass the model's 95% probability interval.

Table 1
Age model tie points for the core HER-GC-UB6. Dating method, tie point core depth (cm), ^{14}C calendar age (yr BP), calendar year and age uncertainties (2σ errors) are shown.

Dating method	Core depth (cm)	^{14}C age (yr BP)	Calendar years	Cal BP age ranges (2σ)
AMS ^{14}C/*G. inflata*	3	631 (±28)	303	222–425
AMS ^{14}C/*G. inflata*	14	1560 (±30)	1144	1031–1257
AMS ^{14}C/*G. inflata*	31	2540 (±25)	2233	2121–2330
AMS ^{14}C/*G. inflata*	66	4184 (±27)	4301	4151–4414
AMS ^{14}C/*G. inflata*	117	6251 (±31)	6726	6614–6859
AMS ^{14}C/*G. inflata*	135	6991 (±38)	7505	7415–7590
AMS ^{14}C/*G. inflata*	143	8191 (±40)	8726	8570–8932
AMS ^{14}C/*G. inflata* + *N. pachyderma*	165	9310 (±40)	10,173	9994–10,291
AMS ^{14}C/*N. pachyderma*	189	11,557 (±46)	13,059	12,880–13,219
AMS ^{14}C/*G. inflata*	204	12,613 (±91)	14,165	13,875–14,662
AMS ^{14}C/*N. pachyderma*	223	15,758 (±70)	18,649	18,464–18,811

washed through a 63 μm sieve and then oven dried at 40 °C. Average resolution per sample is 0.5 ka. Samples were divided into equal splits with a microsplitter in order to generate sub-samples of at least 300 benthic foraminifera. In these sub-samples of the >63 μm size fraction, benthic foraminifera were identified at species level and counted. Taxonomic identifications were made using Cimerman and Langer (1991), Sgarrella and Moncharmont Zei (1993), Milker and Schmiedl (2012), and Holbourn et al. (2013). Relative abundances (%) were obtained from census data. Benthic foraminiferal assemblages were established considering only species reaching ≥10% of relative abundance in at least one sample.

Furthermore, benthic foraminifera were divided into three different microhabitats (Table 2): 1) epifauna (0–0.7 cm below the water-sediment interface; BWSI), 2) infauna (>0.7 cm BWSI), and 5) deep infauna (>3 cm BWSI) (Schmiedl et al., 2000).

Finally, the oxygen index (O_2 index) of Schmiedl et al. (2003) was calculated to analyse changes in oxygen content of bottom waters: [HO/(HO + LO) + Div] × 0.5, where HO is the relative abundance of high-oxygen indicators (epifauna and miliolids), LO is the relative abundance of low-oxygen indicators (deep infauna) (Table 2), and Div is the normalised Shannon-Wiener index (H) (Hill, 1973):

$$H = -\sum p_i \ln p_i$$

where p_i is the proportion of the *i*th species and ln is the natural logarithm.

3.3. Stable isotope measurements

For $\delta^{18}O$ and $\delta^{13}C$ stable isotope analyses in core HER-GC-UB6, ~10 individuals of the planktic foraminifer *Globigerina bulloides* from 67 samples, ~2 individuals of the epifaunal-shallow infaunal *Cibicidoides pachyderma* from 83 samples, and ~4 individuals of the

Table 2
Microhabitat preferences of benthic foraminifera from the HER-GC-UB core: epifauna (0–0.7 cm below the water-sediment interface; BWSI), infauna (>0.7 cm BWSI), and deep infauna (>3 cm BWSI).

Microhabitat		
Epifauna	Infauna	Deep infauna
Alabaminella weddellensis	*Amphicoryna scalaris*	*Chilostomella oolina*
Ammonia sp.	*Astrononion stelligerum*	*Evolvocassidulina bradyi*
Anomalinoides minimus	*Bigenerina nodosaria*	*Fursenkoina complanata*
Anomalinoides sp.	*Bolivina alata*	*Fursenkoina subacuta*
Articulina tubulosa	*Bolivina difformis*	*Globobulimina affinis*
Asterigerinata sp.	*Bolivina dilatata*	*Stainforthia fusiformis*
Cassidulina laevigata	*Bolivina plicatella*	
Cassidulina obtusa	*Bolivina pseudoplicata*	
Cibicides refulgens	*Bolivina spathulata*	
Cibicides sp.	*Bolivina striatula*	
Cibicidoides pachyderma	*Bolivina variabilis*	
Cibicidoides wuellerstorfi	*Bolivina* sp.	
Cibicidoides sp.	*Bolivinella seminuda*	
Connemarella rudis	*Brizalina subspinescens*	
Cornuspira sp.	*Bulimina aculeata*	
Discorbinella sp.	*Bulimina marginata*	
Elphidium aculeatum	*Bulimina striata*	
Elphidium sp.	*Bulimina* sp.	
Favulina hexagona	*Cancris auricula*	
Fissurina sp.	*Chilostomella oolina*	
Gavelinopsis praegeri	*Dentalina* sp.	
Globocassidulina subglobosa	*Evolvocassidulina bradyi*	
Gyroidina altiformis	*Fursenkoina complanata*	
Gyroidina orbicularis	*Fursenkoina subacuta*	
Gyroidina umbonata	*Globobulimina affinis*	
Gyroidina sp.	*Haynesina* sp.	
Hansenisca soldanii	*Marginulina* sp.	
Hanzawaia boueana	*Martinottiella communis*	
Hanzawaia sp.	*Melonis affinis*	
Hoeglundina elegans	*Nodosaria* sp.	
Hyalinea balthica	*Nonion* sp.	
Karrerotextularia flintii	*Nonionella iridea*	
Lagena sp.	*Nonionella* sp.	
Lenticulina sp.	*Nonionoides turgidus*	
Miliolinella sp.	*Pseudoclavulina crustata*	
Neolenticulina variabilis	*Pullenia quadriloba*	
Planulina ariminensis	*Robertina translucens*	
Pyrgo depressa	*Siphouvigerina proboscidea*	
Pyrgo oblonga	*Stainforthia fusiformis*	
Pyrgo williamsoni	*Trifarina angulosa*	
Pyrgo sp.	*Trifarina bradyi*	
Quinqueloculina padana	*Uvigerina auberiana*	
Quinqueloculina seminula	*Uvigerina bononiensis*	
Quinqueloculina sp.	*Uvigerina mediterranea*	
Rosalina sp.	*Uvigerina peregrina*	
Siphonina reticulata	*Uvigerina* sp.	
Sphaeroidina bulloides		
Spiroloculina sp.		
Spiroplectinella wrightii		
Textularia sp.		
Triloculina tricarinata		
Triloculina sp.		

shallow infaunal *Uvigerina peregrina* from 85 samples, were picked from the fraction >212 μm. Samples were crushed using two glass slides under the stereo microscope to open foraminiferal chambers and to clean the inner parts of shells. Cleaning consisted of clay removal with 500 μl of methanol in an ultrasonic bath during 30 s. The residual methanol was extracted and samples dried before analyses. The analyses were carried out by isotope-ratio mass spectrometry (IRMS) in a Finnigan-MAT 252 mass spectrometer linked online to a single acid bath Carbon Kiel-II carbonate preparation device at the Scientific and Technological Centres of the University of Barcelona (CCiT-UB). The analytical precision of laboratory standards was better than 0.08‰ for $\delta^{18}O$, and 0.03‰ for $\delta^{13}C$. Calibration to Vienna Pee Dee Belemnite (VPDB) was performed by means of NBS-19 standards (Coplen, 1996).

The $\delta^{18}O$ values of *C. pachyderma* from core HER-GC-UB6 were corrected by adding 0.5‰ in order to adjust them to the *Uvigerina* values (Shackleton, 1974). Following a similar approach than Hoogakker et al. (2014), we calculated a $\delta^{13}C$ gradient between *C. pachyderma* and *U. peregrina* C stable records from core HER-GC-UB6. This gradient might be related to oxygen changes, as it has been shown for the $\delta^{13}C$ gradient between epifauna (*Cibicidoides wuellerstorfi*) and deep infauna (*Globobulimina* spp.). High *C. wuellerstorfi-Globobulimina* spp. $\delta^{13}C$ gradient values indicate higher oxygen content (Hoogakker et al., 2014). Although any calibration exists for the use of the *C. pachyderma-U. peregrina* $\delta^{13}C$ gradient ($\Delta\delta^{13}C_b$) as oxygen proxy and *U. peregrina* has a variable microhabitat (Mojtahid et al., 2010), similar trends between both the $\Delta\delta^{13}C_b$ and the oxygen index based on benthic foraminifera

validate the application of this gradient as ventilation proxy in the present work (see discussion section 5.2).

3.4. Ichnological analysis of core HER-GC-UB6

Ichnological analysis was conducted on high resolution images of the core sections, previously treated according to the method developed by Dorador and Rodríguez-Tovar (2014) (Fig. S2). Trace fossils identification in cores is not an easy matter, being especially harder in modern marine cores. In this sense, the applied method, based on high resolution image treatment by adjustments modification (*levels*, *brightness* and *vibrance*), facilitates the visualization and identification of trace fossils in this kind of sediments as previously tested in cores from IODP Expedition 339 (e.g., Dorador and Rodríguez-Tovar, 2015, 2018 for a recent review; Rodríguez-Tovar and Dorador, 2015).

3.5. Total Organic Carbon (TOC)

Fifty-three sediment samples from the core HER-GC-UB6 and 26 samples from core MD99-2343 were first freeze-dried and homogenized. Then, the carbonate fraction was removed by attacking with HCl. Total Organic Carbon (TOC) content was analysed at the CCiT-UB. Analytical measurements were performed using an elemental organic analyser Thermo EA Flash 1112 (Thermo Scientific) working in standard conditions. The reproducibility of the TOC % measurements was better than 10% based in measurements on sample replicates.

3.6. Additional cores MD95-2043 and MD99-2343

For core MD95-2043, the age of the studied interval is reliably well constrained by the previously established age model (Cacho et al., 1999) based on 21 ^{14}C ages reporting average sedimentation rates of 51.5 cm/ka for the studied interval (Fig. S1). The age model of core MD99-2343 for the studied interval is based on a recently updated version that added 9 extra ^{14}C ages (Català et al., 2019) to the previously established age model based on 10 ^{14}C ages (Frigola et al., 2008). The average sedimentation rate of this core for the studied interval is of 38.2 cm/ka (Fig. S1).

Some benthic foraminiferal data of the size fraction >150 μm from Reguera (2004) were used: 93 samples from core MD95-2043 with a resolution per sample of 0.25 ka, and 80 samples from core MD99-2343 with a resolution per sample of 0.3 ka. In some of these samples, the whole >150 μm size fraction contained less than 100 benthic foraminifera due to the scarce benthic foraminiferal content of these samples. On average, core MD95-2043 contains 5.96 benthic foraminifera per gram of dry sediment (N/g), and core MD99-2343 contains 4.44 N/g (Figs. S1b and S1c). Since some of the relative abundances (%) from these cores were based on less than 100 benthic foraminifera, which is the minimum number of counts to obtain reliable relative abundances (Fatela and Taborda, 2002), they were used only for interpreting major changes in benthic foraminiferal fauna. Furthermore, benthic foraminiferal assemblages from the size fraction >150 μm do not contain small species, which are commonly related to organic carbon fluxes. Therefore, the comparison between the assemblages of the >63 μm fraction from core HER-GC-UB6 with the assemblages of the size fraction >150 μm from the additional cores was done very carefully, comparing only large temporal intervals (pre-ORL, ORL and post ORL) in a qualitative way.

The benthic *C. pachyderma* δ^{13}C records of deep cores MD95-2043 and MD99-2343 were used as additional data. The TOC data from 47 samples from core MD95-2043 were also used in this study.

4. Results

The results of this study have been described and discussed in 4 intervals: 1) the pre-ORL interval (Last Glacial Maximum (LGM) and Heinrich Stadial 1 (HS1)), 2) the early ORL interval (Bølling-Allerød (B/A)), 3) the late ORL interval (Younger Dryas (Y/D) and early Holocene (EH)), and 4) the post-ORL interval (latest EH, middle Holocene (MH) and late Holocene (LH)) (Fig. 2).

4.1. Chronology of core HER-GC-UB6

According to the generated age model, the studied core encompasses the last 24 ka including the Last Glacial Maximum (LGM), the deglaciation (Heinrich Stadial 1, Bølling-Allerød, Younger Dryas) and the Holocene (Fig. 2). The lower part of the studied core (7.5–24 ka) presents the lowest average sedimentation rate (8.8 cm/ka). In the upper part of the core (0–7.5 ka), sedimentation rates increase with average values of 17.2 cm/ka.

4.2. Sediment colour and trace fossils assemblages of core HER-GC-UB6

Some differences in the ichnological pattern and sediment colour can be observed in the studied core sections, with differentiation of three Ichnological Intervals before, during and after the ORL (Fig. S2).

- Ichnological Interval I (pre-ORL, 255 to 205 cm core depth): It presents dominance of light sediments, with some alternations of dark grey coloured sediments. Mottled background is dominant. In several cases, some discrete trace fossils are visible on this mottled background, but it is difficult to provide a conclusive ichnotaxonomical assignation. A significant feature is that all the differentiated discrete traces show convoluted and deformed shapes. Some traces of *Palaeophycus*, *Planolites*, *Thalassinoides*, ?*Asterosoma*, and smaller traces can be differentiated.
- Ichnological Interval II (ORL, 205 to 146 cm core depth): This interval is characterised by darker coloured sediments and a significant change in the appearance, with the disappearance of the "convolute" look. The lower part of this interval (B/A) reveals dominance of mottled background. From this, in the rest of the interval (Y/D, EH), mottled background is not so evident and is characterised by the presence of very small and scarce discrete traces (small *Palaeophycus*, and ?*Chondrites*).
- Ichnological Interval III (post-ORL, 146 to 0 core depth): The lower part of the Interval III (early MH) shows lighter coloured sediments, and is characterised by the increase in the size of traces, new ichnotaxa as *Thalassinoides*, and the mottled appearance. Then, the rest of the Interval III (late MH, LH) shows continuity with light coloured sediments. The lower part shows a more or less mottled appearance in which some discrete traces can be observed, including *Palaeophycus*, *Planolites* and *Thalassinoides*.

4.3. Benthic foraminiferal assemblages, microhabitats and oxygen index of core HER-GC-UB6

All studied samples contained more than 300 benthic foraminifera due to the high benthic foraminiferal abundance in this core with on average 524 N/g (Fig. S1a).

Relative abundances (%) of the dominant species (≥10% in at least one sample) are shown in Fig. 3 Some of these dominant species are depicted in Fig. 4. During the pre-ORL and early ORL intervals, *Cibicidoides pachyderma* and *Nonionella iridea* alternate (Fig. 3a). *Nonionoides turgidus* shows relatively low and stable abundances with a maximum at the HS1 (Fig. 3a). In addition, *Cassidulina laevigata*, *Bolivina dilatata* and *Uvigerina peregrina* have

relatively high abundances throughout the pre-ORL interval (Fig. 3b–d). Furthermore, during the early ORL interval, *Bolivina spathulata* shows its highest values (Fig. 3c). During the late ORL and post-ORL intervals, high abundances of *B. marginata*, *U. peregrina*, *Uvigerina mediterranea*, *Cassidulina obtusa*, *Brizalina subspinescens*, *Melonis affinis* and *Alabaminella weddellensis* are recorded (Fig. 3b, d, e and f).

The distribution of the three microhabitats (epifauna, infauna, deep infauna) (Table 2) is shown in Fig. 5. The epifauna and infauna, which are the most relevant microhabitats (20–80%), show and opposite pattern through the core (Fig. 5a and b). The infauna shows increasing values from the pre-ORL interval to the early ORL interval (Fig. 5b), while higher values of the epifauna are recorded at the middle of the LGM, the MH and LH (Fig. 5a). In addition, there is an important increase in the abundance of deep infauna during the early ORL marking the onset of the ORL (Fig. 5c).

The benthic foraminiferal-derived oxygen index exhibits relative high values during the LGM, which are followed by an important reduction initiated during the HS1, leading to minimum values at the B/A (Fig. 5d). During the ORL interval, a two-step increment of the oxygen index is observed, recuperating relative well-ventilated conditions at the end of the EH. Well-ventilated conditions maintained relatively stable through the MH and early LH. Finally, an important decrease in the oxygen index takes place over the last 2 ka.

4.4. Stable isotope records

4.4.1. Core HER-GC-UB6

The $\delta^{18}O$ records from the planktic foraminifer *G. bulloides*, and the benthic foraminifera *C. pachyderma* and *U. peregrina* have very similar trends showing the heaviest values during the LGM (3‰ for *G. bulloides* and 5‰ for *C. pachyderma* and *U. peregrina*), an isotopic depletion during the last deglaciation (HS1, B/A, Y/D, EH), and stable (for *C. pachyderma* and *U. peregrina*, 2‰) or gradually heavier (for *G. bulloides*, 0–1‰) values during the MH and LH (Fig. 6a and b).

In this study, the $\delta^{13}C$ of the upwelling-related planktic foraminifer *G. bulloides* is used as a proxy for upwelling intensity since this record uses to decrease during upwelling events (Thunnel and Sautter, 1992; Lebreiro et al., 1997; Schiebel and Hemleben, 2017). This is the result of the combined effect of upwelled $\delta^{13}C$-depleted and nutrient-rich subsurface waters, with the vital effect of *G. bulloides* that calcifies faster implying higher respiration and more respired ^{12}C-enriched CO_2 during the upwelling season (Naidu and Niitsuma, 2004). The planktic *G. bulloides* $\delta^{13}C$ record (Fig. 6a) shows relatively stable values (around −1‰) during the pre-ORL and early ORL intervals. Then, it shows a marked decrease during the late ORL. Finally, this record shows a relatively rapid increase during the MH until reaching stable values around −0.5‰ during the LH.

The benthic foraminiferal $\delta^{13}C$ signal is influenced by several mechanisms, mainly the global C cycle (0.3–0.5‰ changes), the residence time of the water mass, species-specific vital effects (metabolism) and local processes such as remineralisation of organic matter (Rohling and Cooke, 1999; Schmiedl and Mackensen, 2006; Mackensen, 2008).

The $\delta^{13}C$ of *C. pachyderma* is widely used to reconstruct past changes in bottom water ventilation, with high values being interpreted as indicative of young, well-ventilated bottom waters (Sierro et al., 2005). Well-ventilated conditions are observed during the LGM, which are followed by a continuous reduction in the *C. pachyderma* $\delta^{13}C$ record from the HS1 until the EH, where minimum values are recorded (0.75‰) (Fig. 6c). Afterwards, a slight increase of *C. pachyderma* $\delta^{13}C$ suggests a relative recovery of well-

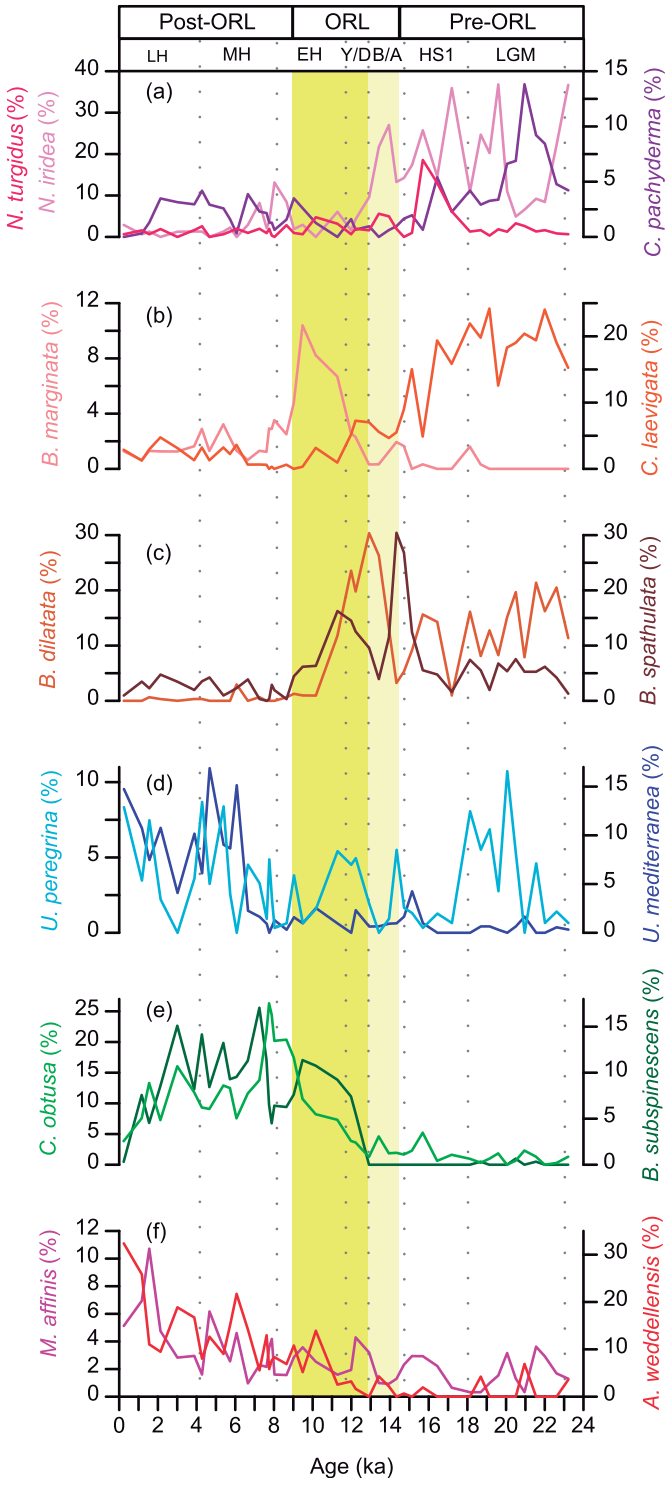

Fig. 3. Relative abundance (%) of dominant and secondary taxa of core HER-GC-UB6 derived from the benthic foraminiferal assemblages: (a) *N. turgidus* (neon red), *N. iridea* (light violet) and *C. pachyderma* (purple); (b) *B. marginata* (sand) and *C. laevigata* (orange); (c) *B. dilatata* (red brown) and *B. spathulata* (dark brown); (d) *U. peregrina* (cyan) and *U. mediterranea* (blue); (e) *C. obtusa* (green) and *B. subspinescens* (forest green); (f) *M. affinis* (pink) and *A. weddellensis* (red). Light yellow vertical bar corresponds to the early ORL interval and dark yellow vertical bar is the late ORL interval. (For interpretation of the references to colour in this figure legend, the reader is referred to the Web version of this article.)

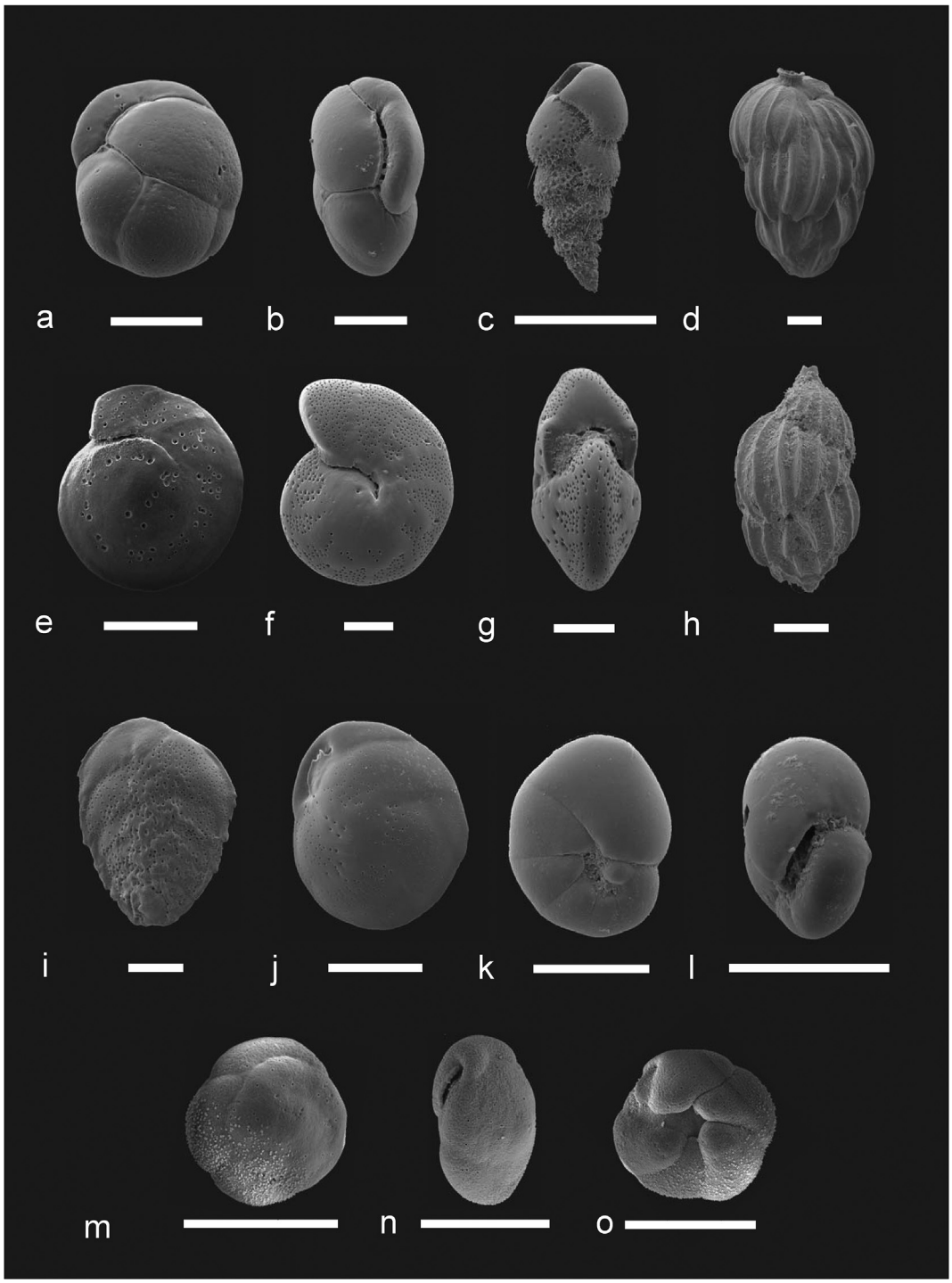

Fig. 4. Most representative benthic foraminiferal species from the core HER-GC-UB6. a) *Cassidulina obtusa*, apertural side; b) *Cassidulina obtusa*, peripheral view; c) *Brizalina subspinescens*, lateral view; d) *Uvigerina mediterranea*, lateral view; e) *Cibicidoides pachyderma*, spiral side; f) *Melonis affinis*, side view; g) *Melonis affinis*, peripheral view; h) *Uvigerina peregrina*, lateral view; i) *Bolivina dilatata*, lateral view; j) *Cassidulina laevigata*, apertural side; k) *Nonionella iridea*, side view; l) *Nonionella iridea*, face view; m) *Alabaminella weddellensis*, spiral side; n) *Alabaminella weddellensis*, peripheral view; o) *Alabaminella weddellensis*, umbilical side. Scale bars = 100 μm.

ventilated bottom water conditions during the post-ORL interval. The benthic $\delta^{13}C$ record of *U. peregrina* (Fig. 6c) has lower values compared to the *C. pachyderma* $\delta^{13}C$ record since the shallow infaunal *U. peregrina* $\delta^{13}C$ reflects the signal of remineralised organic matter in pore waters (McCorkle et al., 1990). This species might be also affected by a negative metabolic effect (vital effect), additionally decreasing $\delta^{13}C$ values (Schmiedl et al., 2004). The *U. peregrina* $\delta^{13}C$ presents relatively high values (−0.5‰) during the pre-ORL and early ORL intervals. A sharp decrease from −0.25 to −0.75‰ is observed at the beginning of the late ORL maintaining lower values (−0.75‰) during the post-ORL interval.

The highest $\Delta\delta^{13}C_b$ gradient values (2‰) observed during the LGM show elevated ventilation conditions (Fig. 6d), coincident with high oxygen index (Fig. 7a). A significant decrease of $\Delta\delta^{13}C_b$

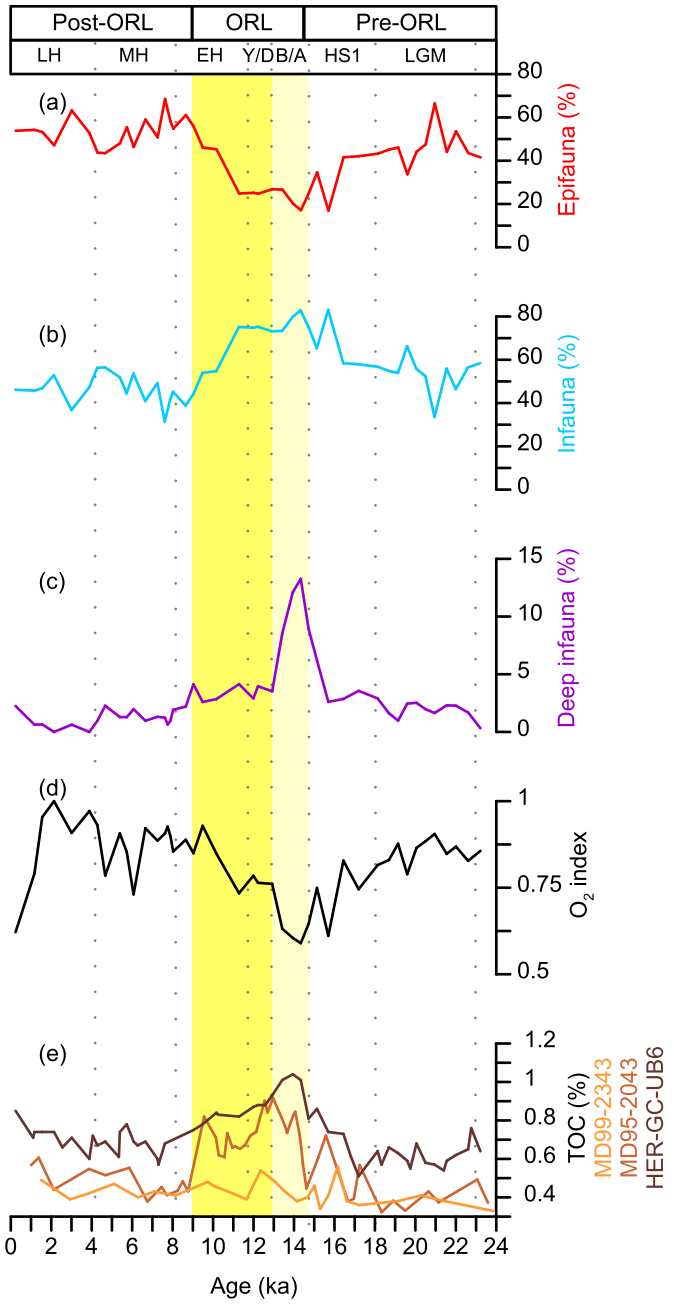

Fig. 5. Microhabitat distribution and oxygen index in core HER-GC-UB6, and TOC records: (a) epifauna (red); (b) infauna (sky blue); (c) deep infauna (purple); (d) oxygen index (black); (e) TOC content (%) from cores HER-GC-UB6 (dark brown), MD95-2043 (red brown) (Cacho et al., 2002), MD99-2343 (light orange). Light yellow vertical bar corresponds to the early ORL interval and dark yellow vertical bar is the late ORL interval. (For interpretation of the references to colour in this figure legend, the reader is referred to the Web version of this article.)

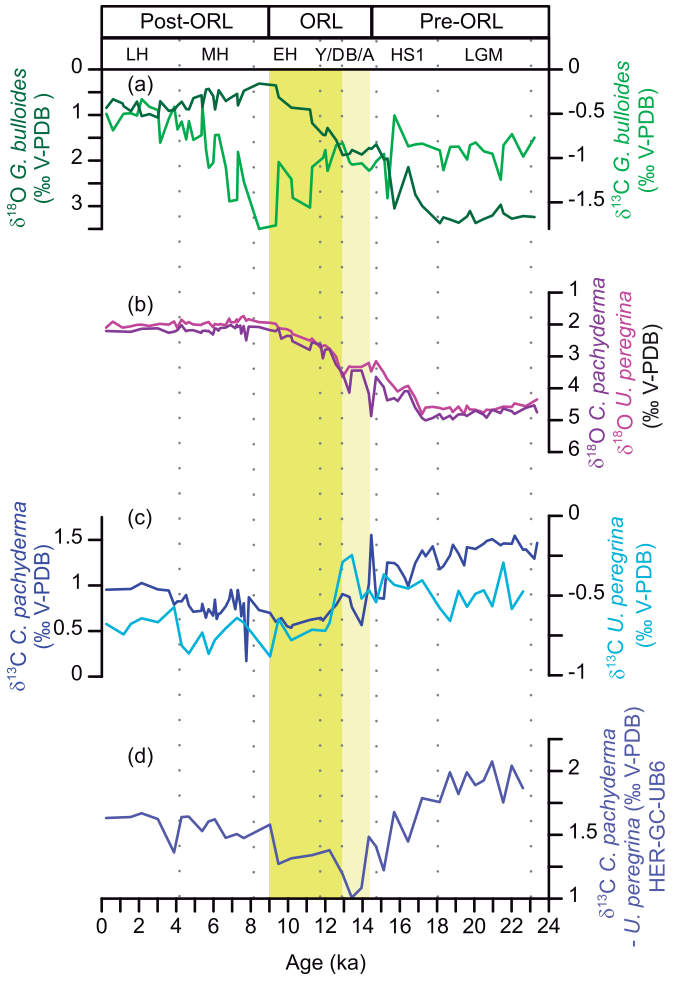

Fig. 6. Foraminiferal $\delta^{18}O$ and $\delta^{13}C$ stable isotope records from core HER-GC-UB6: (a) *G. bulloides* $\delta^{18}O$ (forest green) and *G. bulloides* $\delta^{13}C$ (spring green) records; (b) *C. pachyderma* (purple) and *U. peregrina* (magenta) $\delta^{18}O$ records; (c) *C. pachyderma* (blue) and *U. peregrina* (sky blue) $\delta^{13}C$ records; (d) $\delta^{13}C$ *C. pachyderma-U. peregrina* gradient (electric blue). Light yellow vertical bar corresponds to the early ORL interval and dark yellow vertical bar is the late ORL interval. (For interpretation of the references to colour in this figure legend, the reader is referred to the Web version of this article.)

gradient and oxygen index from HS1 to the early ORL interval indicate a progressive ventilation deterioration (Fig. 7a). Finally, similar to the oxygen index, the $\Delta\delta^{13}C_b$ gradient shows a two-step increase during the late ORL interval, and maintains relatively constant values around 1.6‰ during the post-ORL interval (Fig. 7a).

4.5. Ecological benthic foraminiferal groups

In order to reconstruct bottom water ventilation at different depths, new benthic foraminiferal data from intermediate core HER-GC-UB6 (946 m) (this work), and published benthic foraminiferal data from deep cores, MD95-2043 (1841 m) and MD99-2343 (2391 m) (Reguera, 2004), are presented into three ecological groups recording different oxygen conditions (Schmiedl et al., 2003): 1) high oxygen taxa (epifaunal taxa + miliolids + other oxic species), 2) low oxygen taxa (deep infaunal taxa), and 3) reventilation events (opportunistic taxa *Gyroidina* spp. (Schmiedl et al., 2003)) (Fig. 7e–g). The first ecological group (high oxygen taxa) diminishes along the pre-ORL interval in both intermediate and deep levels (Fig. 7e). Subsequently, during the early ORL interval, the second group (low oxygen taxa) increases in both intermediate and deep cores (Fig. 7f). During the late ORL interval, low oxygen taxa values decrease in the intermediate core while remaining relatively high in the deep Alboran core (MD95-2043) (Fig. 7f). The third group (*Gyroidina* spp.) is dominant during the post-ORL interval, showing similar trends for all three cores (Fig. 7g). This group abundance sharply increases after the ORL, and diminishes gradually afterwards.

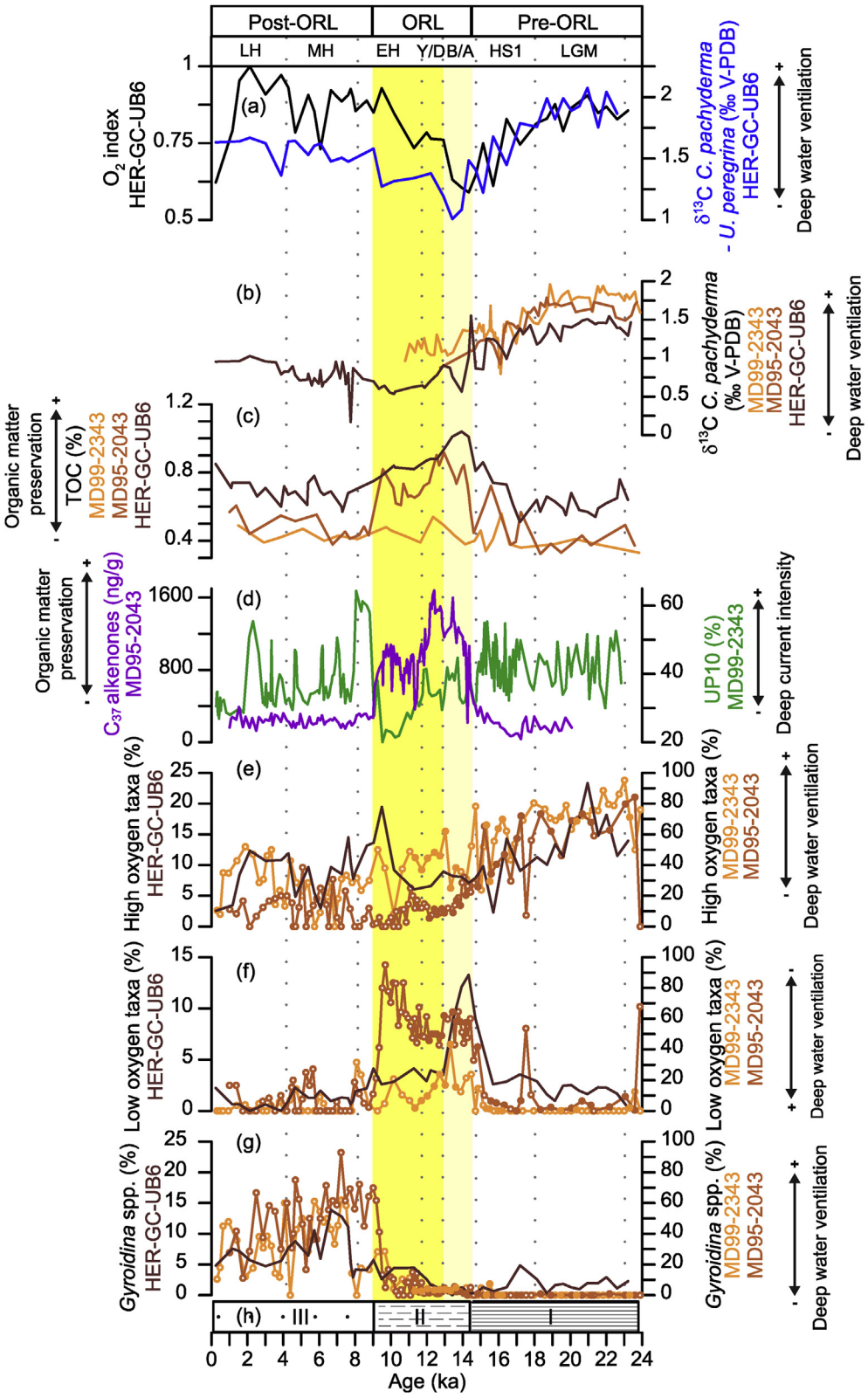

Fig. 7. (a) O_2 index (black) and $\delta^{13}C$ *C. pachyderma-U. peregrina* gradient (electric blue) from core HER-GC-UB6; (b) *C. pachyderma* $\delta^{13}C$ records from cores HER-GC-UB6 (dark brown), MD95-2043 (red brown), MD99-2343 (light orange); (c) TOC content (%) from cores HER-GC-UB6 (dark brown), MD95-2043 (red brown) (Cacho et al., 2002), MD99-2343 (light orange); (d) C_{37} alkenone concentration (ng/g) (purple) (Cacho et al., 2002) and percentage of the UP10 fraction (size fraction >10 μm) from core MD99-2343 (grass green) (Frigola et al., 2008); (e) high oxygen taxa (%) from cores HER-GC-UB6 (dark brown), MD95-2043 (red brown), MD99-2343 (light orange); (f) low oxygen taxa (%) from cores HER-GC-UB6 (dark brown), MD95-2043 (red brown), MD99-2343 (light orange); (g) *Gyroidina* spp. (%) from cores HER-GC-UB6 (dark brown), MD95-2043 (red brown), MD99-2343 (light orange); (h) Ichnological Intervals (I, II, III). In the ecological groups of cores MD95-2043 and MD99-2343 (panels e, f, g), closed dots are percentages based on >100 foraminiferal counts and open dots are percentages based on <100 foraminiferal counts. Ecological groups of core HER-GC-UB6 are based on >300 foraminiferal counts. Light yellow vertical bar

4.6. Total Organic Carbon (TOC) contents

The Total Organic Carbon (TOC) content in marine sediments records the percentage of accumulated organic carbon, which mainly depends on organic matter fluxes and preservation of deposited organic matter (Cacho et al., 2000). The new TOC record from core HER-GC-UB6 highly reproduces, with slightly higher values, the same trend described by the published TOC record (Cacho et al., 2002) of deeper core MD95-2043 (Figs. 5e and 7c). Both records from the Alboran Sea mark the deposition of the ORL, and maximum values are coincident with higher values of published alkenones concentration data (Cacho et al., 2002) in the deepest core between 14.35 and 8.9 ka (Fig. 7d). However, the increase in TOC content is much more gradual in both cores, beginning during the HS1, than the increase shown by alkenones. In the deep core MD99-2343 from the Minorca Rise, a new TOC record shows stable low values around 0.4% indicating that the ORL formation was apparently exclusive of the Alboran Sea and not a general feature of the western Mediterranean Sea (Figs. 5e and 7c). The TOC records of both cores HER-GC-UB6 and MD95-2043 show an opposite trend to the oxygen index (Fig. 7a and c). This result suggests that organic matter accumulation in the Alboran Sea is principally controlled by preservation/oxidation of organic matter.

5. Discussion

5.1. Organic matter fluxes to the sea floor at intermediate depths in the Alboran Sea

Changes in the organic matter input to the sea floor is one of the key environmental factors governing benthic foraminiferal species distribution and abundance, and together with organic matter oxidation, control the accumulation of organic matter at the sea floor (Jorissen et al., 2007). The $\delta^{13}C$ record of shallow infaunal foraminiferal species such as *U. peregrina* reflects changes in the remineralisation rates of organic matter within pore waters. In addition, this species could be also recording a metabolic effect (vital effect) decreasing $\delta^{13}C$ values. The higher remineralisation rates, the lower shallow infauna foraminiferal $\delta^{13}C$ values (McCorkle et al., 1990). Our results from benthic foraminiferal assemblages and *U. peregrina* $\delta^{13}C$ record from core HER-GC-UB6 suggest changes in organic matter fluxes and oxidation/remineralisation of organic matter at intermediate depths in the Alboran Sea at times of deposition of the ORL with an increase in organic fluxes during the late ORL (see below).

The dominance of infaunal and opportunistic taxa able to feed from both fresh and degraded organic matter (*B. dilatata*, *N. iridea*, *B. spathulata*, *U. peregrina*) in the pre-ORL and early ORL intervals supports the development of a mesotrophic environment with episodic (seasonal) organic matter fluxes to the sea floor (Schmiedl et al., 2003, 2010; Diz and Francés, 2008; Duchemin et al., 2008; Koho et al., 2008; Goineau et al., 2012; Pérez-Asensio et al., 2014; Duffield et al., 2015) (Figs. 3 and 5b). The epifaunal-shallow infaunal and opportunistic *C. laevigata*, showing its highest abundances in this interval (Fig. 3b), also inhabits mesotrophic settings with significant seasonal inputs of fresh organic carbon (De Rijk et al., 2000; Morigi et al., 2001; Jones, 2011). This species is also common during glacial times (Schmiedl et al., 1998; Almogi-Labin et al., 2000). These overall mesotrophic conditions along the pre-ORL and early ORL intervals experienced moderate oscillations in the organic matter supply, as is suggested by the alternation of *N. iridea* and *C. pachyderma* (Fig. 3a). Since *C. pachyderma* inhabits oligotrophic environments (Schmiedl et al., 2000, 2003; Pérez-Asensio et al., 2012, 2017), the alternating and opposite trends between *N. iridea* and *C. pachyderma*, might record subtle oscillations between higher and lower organic matter fluxes, respectively (Fig. 3a).

Furthermore, during the pre-ORL (LGM, HS1), but also the early ORL (B/A) intervals, relatively high values of the *U. peregrina* $\delta^{13}C$ record points to lower remineralisation of the organic matter (McCorkle et al., 1990) and, thus, relatively low organic matter fluxes compared to the eutrophic late ORL and post-ORL intervals (Fig. 6c). All these results suggest that organic matter fluxes to the sea floor at the Alboran Sea were episodic (seasonal) and moderate during the 24–13 ka time-interval, i.e. the pre-ORL and the early-ORL (Fig. 8a and b). These observations are consistent with the relatively low concentrations of TOC during the pre-ORL interval but appear contradictory with the observed early ORL high TOC contents. Furthermore, the early ORL record of *U. peregrina* $\delta^{13}C$ maintains relatively high values and *N. iridea* shows high concentrations comparable to the pre-ORL interval. This situation supports the prevalence of mesotrophic conditions thus questioning an enhancement of organic matter flux as the main driver of the initial ORL formation.

During the late ORL interval (Y/D, EH), the *U. peregrina* $\delta^{13}C$ record shows relatively low values (Fig. 6c), suggesting enhanced remineralisation of organic matter in the pore waters (McCorkle et al., 1990), which would imply an increase in organic matter fluxes and/or higher oxygen content. This situation is consistent with the increase in benthic species blooming with high organic matter inputs such as *B. dilatata*, *B. spathulata,* and *B. marginata* (De Rijk et al., 2000; Schmiedl et al., 2000, 2003; Mojtahid et al., 2009; Pérez-Asensio and Aguirre, 2010; Goineau et al., 2012) (Fig. 3), and the increase in the values of the oxygen index and the *C. pachyderma-U. peregrina* $\delta^{13}C$ gradient (Fig. 7a). Moreover, the increase of *B. subspinescens* and *C. obtusa* points to continuous food supply derived from sustained primary productivity (Rathburn and Corliss, 1994; Diz et al., 2007; Bubenshchikova et al., 2015). Therefore, both benthic foraminiferal and *U. peregrina* $\delta^{13}C$ data indicate eutrophic conditions with high sustained organic matter fluxes during the late ORL interval. Local marine primary productivity pulses, riverine discharge, and influx of nutrient-rich Atlantic waters have been proposed as possible organic matter sources for this interval (Y/D, EH) (Jiménez-Espejo et al., 2008; Rodrigo-Gámiz et al., 2011; Ausín et al., 2015a). According to our data, the significant decrease in the *G. bulloides* $\delta^{13}C$ record during this period (Fig. 6a) might reflect increasing intensity of upwelling events possibly related to changes in the Alboran gyres location and/or intensity (Fig. 8c) (Thunnel and Sautter, 1992; Lebreiro et al., 1997; Schiebel and Hemleben, 2017). Nonetheless, higher influx of nutrient-rich Atlantic waters in a context of warming and deglacial sea level rise cannot be ruled out (Ausín et al., 2015a).

During the post-ORL interval (latest EH, MH, LH), the *U. peregrina* $\delta^{13}C$ record maintaining relatively low values (Fig. 6c), along with high abundances of *A. weddellensis*, *C. obtusa*, *B. subspinescens*, *U. mediterranea*, *U. peregrina,* and *M. affinis* (Fig. 3), indicate the permanence of eutrophic conditions with high sustained organic matter fluxes (Fig. 8d) (Rathburn and Corliss, 1994; De Rijk et al., 2000; Schmiedl et al., 2003, 2010; Diz et al., 2007; Bubenshchikova et al., 2015). The combination of species feeding from fresh organic matter (phytodetritus) (*A. weddellensis, U. mediterranea*) (Gooday and Lambshead, 1989; Gooday, 1993; De

corresponds to the early ORL interval and dark yellow vertical bar is the late ORL interval. (For interpretation of the references to colour in this figure legend, the reader is referred to the Web version of this article.)

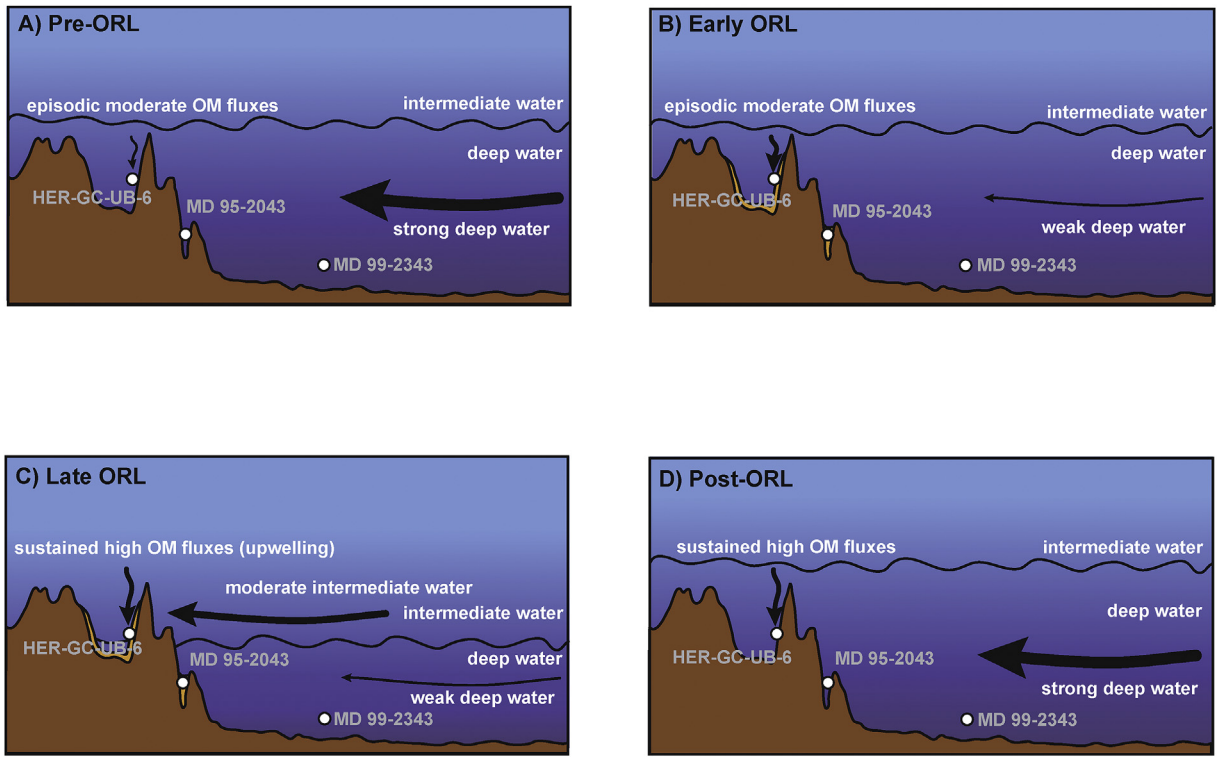

Fig. 8. Proposed intermediate and deep water circulation and organic matter fluxes changes across the ORL: (a) pre-ORL interval, strong deep water circulation and episodic moderate organic matter fluxes; (b) early ORL interval, week deep water circulation and episodic moderate organic matter fluxes; (c) late ORL interval, moderate intermediate water circulation, week deep water circulation and sustained high organic matter fluxes derived from upwelling events; (d) post-ORL interval, strong deep water circulation and sustained high organic matter fluxes. The ORL is coloured in orange in (b) and (c). (For interpretation of the references to colour in this figure legend, the reader is referred to the Web version of this article.)

Rijk et al., 2000; Schmiedl et al., 2003; Fontanier et al., 2006; Diz et al., 2007) with species capable of feeding from refractory organic matter (*M. affinis*) (Schmiedl et al., 2000; Fontanier et al., 2006) is consistent with a sustained high organic matter flux allowing fresh organic matter to remineralise during downward transport along the water column (Westrich and Berner, 1984). Phytodetritus feeders would bloom with the arrival of the first organic particles and species feeding from degraded organic matter would feed from the remineralised organic particles. Since river runoff was reduced (Rodrigo-Gámiz et al., 2011), the origin of this sustained high organic matter supply could be related to the semi-permanent high-productivity 'Málaga cell', which forms due to the southward migration of the Atlantic Jet fostering upwelling of nutrient-rich waters (Sarhan et al., 2000; Ausín et al., 2015b). However, the decreasing *G. bulloides* $\delta^{13}C$ values indicates a gradual reduction in upwelling intensity over the MH (Fig. 6a).

5.2. Deep and intermediate water circulation across the last ORL

The integrated study of the benthic foraminiferal assemblages, benthic $\delta^{13}C$, TOC and ichnological facies provide a solid base to unravel changes in deep water ventilation. These changes would always be overprinted by the above described changes in organic matter fluxes. Nevertheless, the integrated analysis of sites at different depths, under different productivity regimes and using a set of proxies with different sensitivity to organic matter fluxes and deep water ventilation, can provide a solid insight into western Mediterranean changes in deep water ventilation.

One of the most outstanding results from the combination of taxonomic and geochemical analyses on benthic foraminifera is the good agreement between the two independently estimated records of past changes in oxygen content at intermediate depths (HER-GC-UB6; 946 m depth). Both the O_2 index and *C. pachyderma-U. peregrina* $\delta^{13}C$ gradient records show a remarkable decrease in oxygen content coincident with the onset of the ORL deposition, a ventilation recovery during late ORL, and relatively well-oxygenated conditions before and after the ORL deposition (Fig. 7a). It could be argued that minimum O_2 values during the early ORL deposition reflect enhanced organic matter fluxes as is supported by the TOC records and the higher resolution C_{37} alkenones concentration record (Cacho et al., 2002) (Fig. 7c and d). Nevertheless, maximum development of eutrophic conditions with sustained high organic matter fluxes occurred during the late ORL, according to the benthic foraminiferal assemblages and shallow infaunal $\delta^{13}C$ values (see discussion in previous section 5.1). Thus, minimum values in our two O_2 reconstructions (O_2 index and $\delta^{13}C$ gradient) during the early ORL need to have an additional factor to the remineralisation of organic matter provided by organic matter fluxes.

Weaker deep-water ventilation conditions in the western Mediterranean basin could account for minimum O_2 content, a situation supported by the three *C. pachyderma* $\delta^{13}C$ records from intermediate and deep sites (Fig. 7b). All three records show a parallel depletion in $\delta^{13}C$ ratios during the HS1 reaching low values during the early ORL interval. Core MD95-2043 from the western Alboran Sea (1841 m) and core MD99-2343 from the Minorca Rise (2391 m) are located under very different productivity regimes (Fig. 1), and TOC reconstruction from the Minorca core, a rather oligotrophic region, does not show the formation of any ORL but it has a comparable isotopic depletion. This observation supports a weakening in deep convection of the Gulf of Lion as the main driver for the O_2-depletion during the onset of the deglaciation. This

situation is further supported by the coeval reduction in UP10 (size fraction >10 μm) values from the deep site in the Minorca Rise (MD99-2343; Fig. 7d) since this grain-size proxy at this location reflects changes in the intensity of deep water currents (Frigola et al., 2007; Cisneros et al., 2019). Higher ventilation during the pre-ORL interval and reduced ventilation during the early ORL at both intermediate and deep sites is also shown by decreasing high oxygen taxa and increasing low oxygen taxa (Fig. 7e and f). Furthermore, the replacement of Ichnological Interval I (generalized mottled background, convoluted shape, revealing a complete mixing of the shallowest sediment by an important benthic activity) by Ichnological Interval II (darker colour sediments, disappearance of the mottled background, and very small and scarce discrete traces of *Palaeophycus*, and *Chondrites*, revealing decreasing benthic activity) suggests a ventilation decrease during the early ORL (Rodríguez-Tovar et al., 2009a, 2009b; Rodríguez-Tovar and Uchman, 2010, 2011; Monaco et al., 2012; Rodríguez-Tovar and Reolid, 2013) (Fig. 7h and Fig. S2). Geochemical data based on U/Th XRF data from another Alboran site at 2382 m depth also support an oxygen decrease before the ORL deposition (Jiménez-Espejo et al., 2015). These conditions favoured the increase in preservation of organic matter in the Alboran Sea from the pre-ORL to early ORL intervals (Fig. 7c).

During the early ORL, poorly ventilated conditions might be mainly driven by weak deep-water circulation due to higher water column stratification associated with deglacial sea level rise and the subsequent reduction of WMDW formation (Rogerson et al., 2008). Consequently, reduced deep-water circulation lead to higher preservation of organic matter and formation of the ORL in the Alboran Sea, as recorded at different depths (Cacho et al., 2002; Rogerson et al., 2008; Ausín et al., 2015a; Martinez-Ruiz et al., 2015). In summary, the benthic foraminiferal assemblage and *C. pachyderma* $\delta^{13}C$ comparison from intermediate and deep sites (Fig. 7b, e and f) support a parallel and rapid change from glacial-well to deglacial-poor ventilated conditions affecting the water column up to 946 m depth. This situation would have affected the whole western Mediterranean basin although the ORL apparently only formed in the Alboran Sea, likely as a result of the more eutrophic character of this area (Fig. 8a and b).

Interestingly, the benthic foraminiferal assemblage comparison from the deep (1841 m and 2391 m) and intermediate (946 m) sites shows a different behaviour during the second part of the ORL. Diminishing abundances of the deep-infaunal low oxygen taxa group at the intermediate depths (Fig. 7f) indicates an O_2 recovery also supported by the two O_2 reconstructions (Fig. 7a). This observation marks the development of different ventilation behaviour between deep and intermediate depths. Minimum ventilation conditions at the deeper sites are supported by the disappearance of the epifaunal and high-oxygen species *C. pachyderma* during this time, which accounts for the $\delta^{13}C$ record interruption, while this species continues at the intermediate site (Fig. 7b). Furthermore, low oxygen taxa abundances remain relatively high at deep site of the Alboran Sea during the late ORL supporting weak deep ventilation (Fig. 7f). Minimum in deep water currents during this second phase of the ORL are also reported by the UP10 record from the Minorca Rise (Fig. 7d). This decoupled response of intermediate and deep conditions suggests the arrival of better ventilated "intermediate" water mass that would account for the enhanced O_2 arrival at the depth of core HER-GC-UB6 (946 m). This is illustrated in Fig. 8c with the location of a deep-intermediate water mass interphase between the studied intermediate and deep sites. Consequently, the increase of the intermediate water circulation in the Alboran Sea during this period might be related to the reinforcement of intermediate water masses, i.e. LIW (Millot, 2009, 2014), and/or the formation of an intermediate water mass in the Gulf of Lion. On one hand, increased stratification of the water column due to deglacial sea level rise during the second part of the deglaciation likely hinder deep convection in the Gulf of Lion as can be deduced from minimum values of the UP10 proxy north of Minorca (Fig. 7d). On the other hand, reinforcement of LIW ventilation during the YD, which was recorded by grain-size records from Corsica Trough, might have contributed to the first reventilation step at intermediate depths in Alboran Sea, although a rapid reduction of LIW ventilation is also recorded during the early Holocene (Toucanne et al., 2012). In fact, cold and arid conditions during the Y/D (Bárcena et al., 2001; Cacho et al., 2002; Rodrigo-Gámiz et al., 2011; Bartolomé et al., 2015) would likely favoured WMDW formation in the Gulf of Lion.

The ORL ended with a major re-ventilation phase at both intermediate and deep levels as is indicated by the abrupt increase in the opportunistic and indicative of well-ventilated conditions *Gyroidina* spp. group (Schmiedl et al., 2003) for all the studied sites at the same time that deep-water current proxy (UP10) peaked maximum speed values (Fig. 7d). This is consistent with the high O_2 values reached at this time by our two O_2 reconstructions and the Ichnological Interval III reflecting better ventilation (larger trace fossils, mottled appearance, *Palaeophycus*, *Planolites* and *Thalassinoides*) (Rodríguez-Tovar et al., 2009a, 2009b; Rodríguez-Tovar and Uchman, 2010, 2011; Monaco et al., 2012; Rodríguez-Tovar and Reolid, 2013) (Fig. 7a and h). Moreover, poor preservation of organic matter (low TOC) (Fig. 7c) in the Alboran sites is consistent with enhanced ventilation conditions at both intermediate and deep depths (Fig. 8d). This situation denotes the re-establishment of a relative well-ventilated deep circulation in the Western Mediterranean basin after sea level rise and stabilization (Frigola et al., 2007) (Fig. 8d). According to the available chronologies, this reventilation occurred between 9.2 and 7.6 ka, thus predated the eastern Mediterranean reventilation phase that started at 6.1 ka (De Lange et al., 2008) and finalised the last sapropel formation. These observations indicate a rather independence on the operation mode of the thermohaline systems of the two Mediterranean basins during the deglaciation and early-middle Holocene.

6. Conclusions

Benthic foraminiferal assemblages, benthic shallow infaunal $\delta^{13}C$ and *G. bulloides* $\delta^{13}C$ records from intermediate depths at the Alboran Sea recorded changes in organic matter fluxes to the sea floor across the last 24 ka. The pre-ORL (LGM, HS1) and early ORL (B/A) intervals were characterised by mesotrophic conditions with episodic (seasonal) moderate organic matter fluxes. During the late ORL interval (Y/D, EH), organic matter fluxes increased and eutrophic conditions with sustained organic matter supply were established. We posit that increasingly higher intensity of upwelling events, as shown by the decreasing *G. bulloides* $\delta^{13}C$ values, was the source for organic matter fluxes over this interval. During the post-ORL interval (latest EH, MH, LH), similar benthic foraminiferal species and shallow infaunal $\delta^{13}C$ values to those of the late ORL interval point to eutrophic conditions with sustained high organic matter fluxes.

Deep- and intermediate-water circulation variability in the western Mediterranean basin is studied combining benthic foraminiferal assemblages, benthic $\delta^{13}C$, TOC and ichnological facies from three cores covering intermediate and deep depths. The combined application of O_2 indexes from both benthic foraminifera and $\delta^{13}C$ *C. pachyderma-U. peregrina* gradient proves their suitability as reliable oxygen proxies. During the pre-ORL and early ORL intervals, faunal, geochemical and grain-size data show a fast change from glacial-well to deglacial-poor ventilated conditions at both intermediate and deep sites. Since organic fluxes increased

during the Y/D after the beginning of the ORL in the Alboran Sea, the ORL onset was mainly triggered by weak deep-water circulation leading to higher organic matter preservation. During the late ORL, intermediate- and deep-water ventilation are decoupled with enhanced intermediate-water circulation and weak deep-water circulation. This palaeoceanographic interpretation suggests that intermediate depths were bathed by a better-ventilated "intermediate" water mass, which might be related to a more intense or deeper arrival LIW, and/or the formation of an intermediate water mass in the Gulf of Lion. An important reorganization of the water mass structure of the western Mediterranean basin during the deglaciation may account for these circulation changes. The demise of the ORL (post-ORL interval) is marked by better ventilation in both deep and intermediate sites in the western Mediterranean Sea. This reventilation phase (9.2–7.6 ka) predates the eastern Mediterranean reventilation (6.1 ka) that ended the Sapropel 1 deposition, which implies a decoupling between the western and eastern Mediterranean thermohaline systems.

Acknowledgments

We thank the constructive comments of three anonymous reviewers that substantially improved this manuscript. This work was funded by the projects TIMED (Call ref: ERC-CoG-2015; proposal number 683237) of the European Research Council (Consolidator Grants), CHIMERA (CTM2016-75411-R), CGL2015-66835-P and RTI2018-099489-B-I00 of the Ministerio de Economía y Competitividad of Spain. The Research Group GRC Geociències Marines (2017 SGR 315) of the Generalitat de Catalunya is also acknowledged, as well as the Research Groups RNM-178 and RNM-190 (Junta de Andalucía). JNPA has been funded by a Postdoctoral fellowship Beatriu de Pinós funded by the AGAUR from the Generalitat de Catalunya and the European Union through the Marie Curie-COFUND actions. LDP acknowledges support from the Ramón y Cajal program (MINECO, Spain), JF from the Serra Húnter Programme (Generalitat de Catalunya) and IC from the ICREA-Academia program from the Generalitat de Catalunya. We are indebted to Albert Català and Montse Guart (University of Barcelona), and Joaquim Perona and Regina Roca (CCiT-UB) for their support with the laboratory work.

Appendix A. Supplementary data

Supplementary data to this article can be found online at https://doi.org/10.1016/j.quascirev.2019.106075.

References

Aguirre, J., Gibert, J.M., Puga-Bernabeu, A., 2010. Proximal-distal ichnofabric changes in a siliciclastic shelf, early Pliocene, Guadalquivir basin, southwest Spain. Palaeogeogr. Palaeoclimatol. Palaeoecol. 291, 328–337. https://doi.org/10.1016/j.palaeo.2010.03.004.

Almogi-Labin, A., Schmiedl, G., Hemleben, C., Siman-Tov, R., Segl, M., Meischner, D., 2000. The influence of the NE winter monsoon on productivity changes in the Gulf of Aden, NW Arabian Sea, during the last 530 ka as recorded by foraminifera. Mar. Micropaleontol. 40, 295–319. https://doi.org/10.1016/S0377-8398(00)00043-8.

Asper, V.L., Deuser, W., Knauer, G., Lohrenz, S., 1992. Rapid coupling of sinking particle fluxes between surface and deep ocean waters. Nature 357, 670–672. https://doi.org/10.1038/357670a0.

Ausín, B., Flores, J.-A., Sierro, F.-J., Bárcena, M.-A., Hernández-Almeida, I., Francés, G., Gutiérrez-Arnillas, E., Martrat, B., Grimalt, J.O., Cacho, I., 2015a. Coccolithophore productivity and surface water dynamics in the Alboran Sea during the last 25 kyr. Palaeogeogr. Palaeoclimatol. Palaeoecol. 418, 126–140. https://doi.org/10.1016/j.palaeo.2014.11.011.

Ausín, B., Flores, J.A., Sierro, F.J., Cacho, I., Hernández-Almeida, I., Martrat, B., Grimalt, J.O., 2015b. Atmospheric patterns driving Holocene productivity in the Alboran Sea (western mediterranean): a multiproxy approach. Holocene 25, 1–13. https://doi.org/10.1177/0959683614565952.

Bakun, A., 1990. Global climate change and intensification of coastal ocean upwelling. Science 247, 198–201. https://doi.org/10.1126/science.247.4939.198.

Bárcena, M.A., Cacho, I., Abrantes, F., Sierro, F.J., Grimalt, J.O., Flores, J.A., 2001. Paleoproductivity variations related to climatic conditions in the Alboran Sea (western Mediterranean) during the last glacial-interglacial transition: the diatom record. Palaeogeogr. Palaeoclimatol. Palaeoecol. 167, 337–357. https://doi.org/10.1016/S0031-0182(00)00246-7.

Bartolomé, M., Moreno, A., Sancho, C., Stoll, H.M., Cacho, I., Spötl, C., Belmonte, Á., Edwards, R.L., Cheng, H., Hellstrom, J.C., 2015. Hydrological change in southern Europe responding to increasing north Atlantic overturning during Greenland Stadial 1. Proc. Natl. Acad. Sci. U. S. A 112, 6568–6572. www.pnas.org/cgi/doi/10.1073/pnas.1503990112.

Béthoux, J.P., 1980. Mean water fluxes across sections in the Mediterranean Sea, evaluated in the basis of water and salt budgets and of observed salinities. Oceanol. Acta 3, 79–88.

Blaauw, M., Christen, J.A., 2011. Bacon manual – v2, 2, 1–11.

Bryden, H.L., Stommel, H.M., 1984. Limiting processes that determine basic features of the circulation in the Mediterranean Sea. Oceanol. Acta 7, 289–296.

Bubenshchikova, N., Nürnbergb, D., Tiedemann, R., 2015. Variations of Okhotsk Sea oxygen minimum zone: comparison of foraminiferal and sedimentological records for latest MIS 12-11c and latest MIS 2-1. Mar. Micropaleontol. 121, 52–69. https://doi.org/10.1016/j.marmicro.2015.09.004.

Cacho, I., Grimalt, J.O., Pelejero, C., Canals, M., Sierro, F.J., Flores, J.A., Shackleton, N.J., 1999. Dansgaard-oeschger and Heinrich event imprints in Alboran Sea temperatures. Paleoceanography 14, 698–705. https://doi.org/10.1029/1999PA900044.

Cacho, I., Grimalt, J.O., Sierro, F.J., Shackleton, N., Canals, M., 2000. Evidence for enhanced Mediterranean thermohaline circulation during rapid climatic coolings. Earth Planet. Sci. Lett. 183, 417–429. https://doi.org/10.1016/S0012-821X(00)00296-X.

Cacho, I., Grimalt, J.O., Canals, M., 2002. Response of the Western Mediterranean Sea to rapid climatic variability during the last 50,000 years: a molecular biomarker approach. J. Mar. Syst. 33–34, 253–272. https://doi.org/10.1016/S0924-7963(02)00061-1.

Cacho, I., Shackleton, N., Elderfield, H., Sierro, F.J., Grimalt, J.O., 2006. Glacial rapid variability in deep-water temperature and $\delta^{18}O$ from the western Mediterranean Sea. Quat. Sci. Rev. 25, 3294–3311. https://doi.org/10.1016/j.quascirev.2006.10.004.

Català, A., Cacho, I., Frigola, J., Pena, L.D., Lirer, F., 2019. Holocene hydrography evolution in the Alboran Sea: a multi-record and multiproxy comparison. Clim. Past 15, 927–942. https://doi.org/10.5194/cp-15-927-2019.

Cimerman, F., Langer, M.R., 1991. Mediterranean foraminifera. In: Slovenska Akademija Znanosti in Umetnosti. Academia Scientiarum et Artium Slovencia Cl. 4 Hist. Nat., vol. 30 (Ljubljana).

Cisneros, M., Cacho, I., Frigola, J., Sanchez-Vidal, A., Calafat, A., Pedrosa-Pàmies, R., Rumín-Caparrós, A., Canals, M., 2019. Deep-water formation variability in the north-western Mediterranean Sea during the last 2500 yr: a proxy validation with present-day data. Glob. Planet. Change 177, 56–68. https://doi.org/10.1016/j.gloplacha.2019.03.012.

Coplen, T.B., 1996. New guidelines for reporting stable hydrogen, carbon, and oxygen isotope-ratio data. Geochem. Cosmochim. Acta 60, 3359–3360. https://doi.org/10.1016/0016-7037(96)00263-3.

De Lange, G.J., Thomson, J., Reitz, A., Slomp, C.P., Speranza Principato, M., Erba, E., Corselli, C., 2008. Synchronous basin-wide formation and redox-controlled preservation of a Mediterranean sapropel. Nat. Geosci. 1, 606–610. https://doi.org/10.1038/ngeo283.

De Rijk, S., Jorissen, F.J., Rohling, E.J., Troelstra, S.R., 2000. Organic flux control on bathymetric zonation of Mediterranean benthic foraminifera. Mar. Micropaleontol. 40, 151–166. https://doi.org/10.1016/S0377-8398(00)00037-2.

Diz, P., Hall, I.R., Zahn, R., Molyneux, E.G., 2007. Paleoceanography of the southern Agulhas Plateau during the last 150 ka: inferences from benthic foraminiferal assemblages and multispecies epifaunal carbon isotopes. Paleoceanography 22, PA4218. https://doi.org/10.1029/2007PA001511.

Diz, P., Francés, G., 2008. Distribution of live benthic foraminifera in the Ría de Vigo (NW Spain). Mar. Micropaleontol. 66, 165–191. https://doi.org/10.1016/j.marmicro.2007.09.001.

Dorador, J., Rodríguez-Tovar, F.J., 2015. Application of digital image treatment to the characterization and differentiation of deep-sea ichnofacies. Span. J. Palaeontol. 30, 265–673.

Dorador, J., Rodríguez-Tovar, F.J., IODP Expedition 339 Scientists, 2014. Digital image treatment applied to ichnological analysis of marine core sediments. Facies 60, 39–44. https://doi.org/10.1007/s10347-013-0383-z.

Dorador, J., Rodríguez-Tovar, F.J., 2018. High-resolution image treatment in ichnological core analysis: initial steps, advances and prospects. Earth Sci. Rev. 177, 226–237.

Duchemin, G., Jorissen, F.J., Le Loc'h, F., Andrieux-Loyer, F., Hily, C., Thouzeau, G., 2008. Seasonal variability of living benthic foraminifera from the outer continental shelf of the Bay of Biscay. J. Sea Res. 59, 297–319. https://doi.org/10.1016/j.seares.2008.03.006.

Duffield, C.J., Hess, S., Norling, K., Alve, E., 2015. The response of *Nonionella iridea* and other benthic foraminifera to "fresh" organic matter enrichment and physical disturbance. Mar. Micropaleontol. 120, 20–30. https://doi.org/10.1016/j.marmicro.2015.08.002.

Emeis, K.-C., Sakamoto, T., Wehausen, R., Brumsack, H.-J., 2000. The sapropel record of the eastern Mediterranean Sea — results of ocean drilling program leg 160. Palaeogeogr. Palaeoclimatol. Palaeoecol. 158, 371–395. https://doi.org/10.1016/

S0031-0182(00)00059-6.
Fatela, F., Taborda, R., 2002. Confidence limits of species proportions in microfossil assemblages. Mar. Micropaleontol. 45, 169–174. https://doi.org/10.1016/S0377-8398(02)00021-X.
Fontanier, C., Jorissen, F.J., Anschutz, P., Chaillou, G., 2006. Seasonal variability of benthic foraminiferal faunas at 1000 m depth in the Bay of Biscay. J. Foraminifer. Res. 36, 61–76. https://doi.org/10.2113/36.1.61.
Frigola, J., Moreno, A., Cacho, I., Canals, M., Sierro, F.J., Flores, J.A., Grimalt, J.O., Hodell, D.A., Curtis, J.H., 2007. Holocene climate variability in the western Mediterranean region from a deepwater sediment record. Paleoceanography 22, PA2209. https://doi.org/10.1029/2006PA001307.
Frigola, J., Moreno, A., Cacho, I., Canals, M., Sierro, F.J., Flores, J.A., Grimalt, J.O., 2008. Evidence of abrupt changes in Western Mediterranean deep water circulation during the last 50 kyr: a high-resolution marine record from the Balearic Sea. Quat. Int. 181, 88–104. https://doi.org/10.1016/j.quaint.2007.06.016.
García-Gorriz, E., Carr, M.E., 1999. The climatological annual cycle of satellite-derived phytoplankton pigments in the Alboran Sea: a physical interpretation. Geophys. Res. Lett. 26, 2985–2988. https://doi.org/10.1029/1999GL900529.
Gardner, W.D., Southard, J.B., Hollister, C.D., 1985. Sedimentation, resuspension and chemistry of particles in the northwest Atlantic. Mar. Geol. 65, 199–242. https://doi.org/10.1016/0025-3227(85)90057-X.
Gascard, J.C., Richez, C., 1985. Water masses and circulation in the western Alboran Sea and in the straits of Gibraltar. Prog. Oceanogr. 15, 157–216. https://doi.org/10.1016/0079-6611(85)90031-X.
García-Martínez, M.C., Vargas-Yáñez, M., Moya, F., Santiago, R., Muñoz, M., Reul, A., Ramírez, T., Balbín, R., 2019. Average nutrient and chlorophyll distributions in the western Mediterranean: RADMED project. Oceanologia 61, 143–169. https://doi.org/10.1016/j.oceano.2018.08.003.
Goineau, A., Fontanier, C., Jorissen, F., Buscail, R., Kerhervé, P., Cathalot, C., Pruski, A.M., Bourgeois, S., Metzger, E., Legrand, E., Rabouille, C., 2012. Temporal variability of live (stained) benthic foraminiferal faunas in a river-dominated shelf - faunal response to rapid changes of the river influence (Rhône prodelta, NW Mediterranean). Biogeosciences 9, 1367–1388. https://doi.org/10.5194/bg-9-1367-2012.
Gooday, A.J., 1993. Deep-sea benthic foraminiferal species which exploit phytodetritus: characteristic features and controls on distribution. Mar. Micropaleontol. 22, 187–205. https://doi.org/10.1016/0377-8398(93)90043-W.
Gooday, A.J., Lambshead, P.J.D., 1989. Influence of seasonally deposited phytodetritus on benthic foraminiferal populations in the bathyal northeast Atlantic: the species response. Mar. Ecol. Prog. Ser. 58, 53–67.
Heburn, G.W., La Violette, P.E., 1990. Variations in the structure of the anticyclonic gyres found in the Alboran Sea. J. Geophys. Res. 95, 1599–1613. https://doi.org/10.1029/JC095iC02p01599.
Hedges, J.I., Keil, R.G., Benner, R., 1997. What happens to terrestrial organic matter in the ocean? Org. Geochem. 27, 195–212. https://doi.org/10.1016/S0146-6380(97)00066-1.
Hill, M.O., 1973. Diversity and evenness: a unifying notation and its consequences. Ecology 54, 427–432.
Hoogakker, B.A.A., Elderfield, H., Schmiedl, G., McCave, I.N., Rickaby, R.E.M., 2014. Glacial-interglacial changes in bottom-water oxygen content on the Portuguese margin. Nat. Geosci. 8, 40–43. https://doi.org/10.1038/ngeo2317.
Holbourn, A., Henderson, A.S., MacLeod, N., 2013. Atlas of Benthic Foraminifera. Wiley-Blackwell and Natural History Museum, Oxford, UK.
Jiménez-Espejo, F.J., Martínez-Ruiz, F., Rogerson, M., González Donoso, J.M., Romero, O.E., Linares, D., Sakamoto, T., Gallego-Torres, D., Rueda Ruiz, J.L., Ortega Huertas, M., Pérez Claros, J.A., 2008. Detrital input, productivity fluctuations, and water mass circulation in the westernmost Mediterranean Sea since the Last Glacial maximum. Geochem. Geophys. Geosyst. 9, Q11U02. https://doi.org/10.1029/2008GC002096.
Jiménez-Espejo, F.J., Pardos-Gene, M., Martinez-Ruiz, F., Garcia-Alix, A., van de Flierdt, T., Toyofuku, T., Bahr, A., Kreissig, K., 2015. Geochemical evidence for intermediate water circulation in the westernmost Mediterranean over the last 20kyr BP and its impact on the Mediterranean outflow. Glob. Planet. Change 135, 38–46. https://doi.org/10.1016/j.gloplacha.2015.10.001.
Jones, R.W., 2011. Applications of Palaeontology: Techniques and Case Studies. Cambridge University Press, Cambridge.
Jorissen, F.J., de Stigter, H.C., Widmark, J.G.V., 1995. A conceptual model explaining benthic foraminiferal microhabitats. Mar. Micropaleontol. 26, 3–15. https://doi.org/10.1016/0377-8398(95)00047-X.
Jorissen, F.J., Fontanier, C., Ellen, T., 2007. Paleoceanographical proxies based on deep-sea benthic foraminiferal assemblage characteristics. In: Hillaire-Marcel, C., De Vernal, A. (Eds.), Developments in Marine Geology, vol. 1. Elsevier, Amsterdam, pp. 263–325. https://doi.org/10.1016/S1572-5480(07)01006-8.
Kidd, R.B., Cita, M.B., Ryan, W.B.F., 1978. Stratigraphy of eastern Mediterranean sapropel sequences recovered during DSDP Leg 42A and their paleoenvironmental significance. In: Hsü, K.J., Montadert, L., et al. (Eds.), Initial Reports, vol. 42. DSDP, Washington, pp. 421–443.
Koho, K.A., García, R., de Stigter, H.C., Epping, E., Koning, E., Kouwenhoven, T.J., van der Zwaan, G.J., 2008. Sedimentary labile organic carbon and pore water redox control on species distribution of benthic foraminifera: a case study from Lisbon-Setúbal Canyon (southern Portugal). Prog. Oceanogr. 79, 55–82. https://doi.org/10.1016/j.pocean.2008.07.004.
La Violette, P.E., 1986. Short-term measurements of surface currents associated with the Alboran Sea Gyre. J. Phys. Oceanogr. 16, 262–279. https://doi.org/10.1175/1520-0485(1986)016<0262:STMOSC>2.0.CO;2.
Lacombe, H., Tchernia, P., Gamberoni, L., 1985. Variable bottom water in the western Mediterranean basin. Prog. Oceanogr. 14, 319–338. https://doi.org/10.1016/0079-6611(85)90015-1.
Lebreiro, S.M., Moreno, J.C., Abrantes, F.F., Pflaumann, U., 1997. Productivity and paleoceanographic implications on the Tore Seamount (Iberian Margin) during the last 225 kyr: foraminiferal evidence. Paleoceanography 12, 718–727. https://doi.org/10.1029/97PA01748.
Mackensen, A., 2008. On the use of benthic foraminiferal $\delta^{13}C$ in palaeoceanography: constraints from primary proxy relationships. In: Austin, W.E.N., James, R.H. (Eds.), Biogeochemical Controls on Palaeoceanographic Environmental Proxies, vol. 303. Geological Society, London, Special Publications, pp. 121–133.
Malanotte-Rizzoli, P., Artale, V., Borzelli-Eusebi, G.L., Brenner, S., Crise, A., Gacic, M., Kress, N., Marullo, S., Ribera d'Alcalà, M., Sofianos, S., Tanhua, T., Theocharis, A., Alvarez, M., Ashkenazy, Y., Bergamasco, A., Cardin, V., Carniel, S., Civitarese, G., D'Ortenzio, F., Font, J., Garcia-Ladona, E., Garcia-Lafuente, J.M., Gogou, A., Gregoire, M., Hainbucher, D., Kontoyannis, H., Kovacevic, V., Kraskapoulou, E., Kroskos, G., Incarbona, A., Mazzocchi, M.G., Orlic, M., Ozsoy, E., Pascual, A., Poulain, P.-M., Roether, W., Rubino, A., Schroeder, K., Siokou-Frangou, J., Souvermezoglou, E., Sprovieri, M., Tintoré, J., Triantafyllou, G., 2014. Physical forcing and physical/biochemical variability of the Mediterranean Sea: a review of unresolved issues and directions for future research. Ocean Sci. 10, 281–322. https://doi.org/10.5194/os-10-281-2014.
Marshall, J., Schott, F., 1999. Open-ocean convection: observations, theory, and models models. Rev. Geophys. 37, 1–64. https://doi.org/10.1029/98RG02739.
Martinez-Ruiz, F., Kastner, M., Gallego-Torres, D., Rodrigo-Gamiz, M., Nieto-Moreno, V., Ortega-Huertas, M., 2015. Paleoclimate and paleoceanography over the past 20,000 yr in the Mediterranean Sea Basins as indicated by sediment elemental proxies. Quat. Sci. Rev. 107, 25–46. https://doi.org/10.1016/j.quascirev.2014.09.018.
McCorkle, D.C., Keigwin, L.D., Corliss, B.H., Emerson, S.R., 1990. The influence of microhabitats on the carbon isotopic composition of deep-sea benthic foraminifera. Paleoceanography 5, 161–185. https://doi.org/10.1029/PA005i002p00161.
MEDOC Group, 1970. Observation of formation of deep water in the Mediterranean Sea. Nature 227, 1037–1040. https://doi.org/10.1038/2271037a0.
Milker, Y., Schmiedl, G., 2012. A taxonomic guide to modern benthic shelf foraminifera of the western Mediterranean Sea. Palaeontol. Electron. 15 (2), 16A. palaeo-electronica.org/content/2012-issue-2-articles/223-taxonomy-foraminifera.
Millot, C., 1999. Circulation in the western Mediterranean Sea. J. Mar. Syst. 20, 423–442. https://doi.org/10.1016/S0924-7963(98)00078-5.
Millot, C., 2009. Another description of the Mediterranean Sea outflow. Prog. Oceanogr. 82, 101–124. https://doi.org/10.1016/S0924-7963(98)00078-5.
Millot, C., 2014. Heterogeneities of in-and out-flows in the Mediterranean Sea. Prog. Oceanogr. 120, 254–278. https://doi.org/10.1016/j.pocean.2013.09.007.
Mojtahid, M., Jorissen, F., Lansard, B., Fontanier, C., Bombled, B., Rabouille, C., 2009. Spatial distribution of live benthic foraminifera in the Rhône prodelta: faunal response to a continental-marine organic matter gradient. Mar. Micropaleontol. 70, 177–200. https://doi.org/10.1016/j.marmicro.2008.12.006.
Mojtahid, M., Griveaud, C., Fontanier, C., Anschutz, P., Jorissen, F.J., 2010. Live benthic foraminiferal faunas along a bathymetrical transect (140–4800m) in the Bay of Biscay (NE Atlantic). Rev. Micropaleontol. 53, 139–162. https://doi.org/10.1016/j.revmic.2010.01.002.
Monaco, P., Rodríguez-Tovar, F.J., Uchman, A., 2012. Ichnological analysis of lateral environmental heterogeneity within the Bonarelli level (Uppermost Cenomanian) in the classical localities near Gubbio, Central Apennines, Italy. Palaios 27, 48–54. https://doi.org/10.2110/palo.2011.p11-018r.
Morigi, C., Jorissen, F.J., Gervais, A., Guichard, S., Borsetti, A.M., 2001. Benthic foraminiferal faunas in surface sediments off NW Africa: relationship with organic flux to the ocean floor. J. Foraminifer. Res. 31, 350–368. https://doi.org/10.2113/0310350.
Murat, A., 1999. Pliocene–Pleistocene occurrence of sapropels in the Western Mediterranean Sea and their relation to eastern Mediterranean sapropels. In: Zahn, R., Comas, M.C., Klaus, A. (Eds.), Proc. ODP, Sci. Results, vol. 161. Ocean Drilling Program), College Station, TX, pp. 519–527. https://doi.org/10.2973/odp.proc.sr.161.244.1999.
Murray, J.W., 2006. Ecology and Applications of Benthic Foraminifera. Cambridge University Press, Cambridge.
Naidu, P., Niitsuma, N., 2004. Atypical $\delta^{13}C$ signature in *Globigerina bulloides* at the ODP Site 723An (Arabian Sea): implications of environmental changes caused by upwelling. Mar. Micropaleontol. 53, 1–10. https://doi.org/10.1016/j.marmicro.2004.01.005.
Parrilla, G., Kinder, T.H., Preller, R.H., 1986. Deep and intermediate mediterranean water in the western Alboran Sea. Deep-Sea Res. 33, 55–88. https://doi.org/10.1016/0198-0149(86)90108-1.
Pemberton, S.G., Spila, M., Pulham, A.J., Saunders, T., MacEachern, J.A., Robbins, D., Sinclair, I.K., 2001. Ichnology and sedimentology of shallow to marginal marine systems. In: Ben Nevis & Avalon Reservoirs, Jeanne d'Arc Basin. Geological Association of Canada, St. John's.
Pérez-Asensio, J.N., Aguirre, J., 2010. Benthic foraminiferal assemblages in temperate coral-bearing deposits from the Late Pliocene. J. Foraminifer. Res. 40, 61–78. https://doi.org/10.2113/gsjfr.40.1.61.
Pérez-Asensio, J.N., Aguirre, J., Schmiedl, G., Civis, J., 2012. Messinian

paleoenvironmental evolution in the lower Guadalquivir Basin (SW Spain) based on benthic foraminifera. Palaeogeogr. Palaeoclimatol. Palaeoecol. 326–328, 135–151. https://doi.org/10.1016/j.palaeo.2012.02.014.

Pérez-Asensio, J.N., Aguirre, J., Schmiedl, G., Civis, J., 2014. Messinian productivity changes in the northeastern Atlantic and their relationship to the closure of the Atlantic-Mediterranean gateway: implications for Neogene palaeoclimate and palaeoceanography. J. Geol. Soc. Lond. 171, 389–400. https://doi.org/10.1144/jgs2013-032.

Pérez-Asensio, J.N., Aguirre, J., Rodríguez-Tovar, F.J., 2017. The effect of bioturbation by polychaetes (Opheliidae) on benthic foraminiferal assemblages and test preservation. Palaeontology 60, 807–827. https://doi.org/10.1111/pala.12317.

Pinardi, N., Masetti, E., 2000. Variability of the large scale general circulation of the Mediterranean Sea from observations and modelling: a review. Palaeogeogr. Palaeoclimatol. Palaeoecol. 158, 153–173. https://doi.org/10.1016/S0031-0182(00)00048-1.

Quiroz, L.I., Buatois, L.A., Mángano, M.G., Jaramillo, C.A., Santiago, N., 2010. Is the trace fossil Macaronichnus an indicator of temperate to cold waters? Exploring the paradox of its occurrence in tropical coasts. Geology 38, 651–654. https://doi.org/10.1130/G30140.1.

Rathburn, A.E., Corliss, B.N., 1994. The ecology of living (stained) deep-sea benthic foraminifera from the Sulu Sea. Paleoceanography 9, 87–150. https://doi.org/10.1029/93PA02327.

Reguera, M.I., 2004. Respuesta del Mediterráneo Occidental a los cambios climáticos bruscos ocurridos durante el último ciclo glacial: Estudio de las asociaciones de foraminíferos. Ph.D. Thesis. University of Salamanca, Spain. http://oceano.usal.es/wp-content/uploads/sites/30/2019/11/Tesis-MIRG.pdf.

Reimer, P.J., Bard, E., Bayliss, A., Beck, J.W., Blackwell, P.G., Bronk Ramsey, C., Buck, C.E., Edwards, R.L., Friedrich, M., Grootes, P.M., Guilderson, T.P., Haflidason, H., Hajdas, I., Hatté, C., Heaton, T.J., Hömann, D.L., Hogg, A.G., Hughen, K.A., Kaiser, K.F., Kromer, B., Manning, S.W., Niu, M., Reimer, R.W., Richards, D.A., Scott, M.E., Southon, J.R., Turney, C.S.M., van der Plicht, J., 2013. Intcal13 and Marine13 radiocarbon age calibration curves 0-50,000 years cal BP. Radiocarbon 55, 1869–1887. https://doi.org/10.2458/azu_js_rc.55.16947.

Rodrigo-Gámiz, M., Martinez-Ruiz, F., Jiménez-Espejo, F.J., Gallego-Torres, D., Nieto-Moreno, V., Romero, O., Ariztegui, D., 2011. Impact of climate variability in the western Mediterranean during the last 20,000 years: oceanic and atmospheric responses. Quat. Sci. Rev. 30, 2018–2034. https://doi.org/10.1016/j.quascirev.2011.05.011.

Rodríguez-Tovar, F.J., Dorador, J., 2014. Ichnological analysis of Pleistocene sediments from the IODP Site U1385 "Shackleton Site" on the Iberian margin: approaching paleoenvironmental conditions. Palaeogeogr. Palaeoclimatol. Palaeoecol. 409, 24–32. https://doi.org/10.1016/j.palaeo.2014.04.027.

Rodríguez-Tovar, F.J., Dorador, J., 2015. Ichnofabric characterization in cores: a method of digital image treatment. Ann. Soc. Geol. Pol. 85, 465–471. https://doi.org/10.14241/asgp.2015.010.

Rodríguez-Tovar, F.J., Reolid, M., 2013. Environmental conditions during the Toarcian Oceanic Anoxic Event (T-OAE) in the westernmost Tethys: influence of the regional context on a global phenomenon. Bull. Geosci. 88, 697–712. https://doi.org/10.3140/bull.geosci.1397.

Rodríguez-Tovar, F.J., Uchman, A., 2010. Ichnofabric evidence for the lack of bottom anoxia during the lower Toarcian oceanic anoxic event (T-OAE) in the Fuente de la Vidriera section, betic Cordillera, Spain. Palaios 25, 576–587. https://doi.org/10.2110/palo.2009.p09-153r.

Rodríguez-Tovar, F.J., Uchman, A., 2011. Ichnological data as a useful tool for deep-sea environmental characterization: a brief overview and an application to recognition of small-scale oxygenation changes during the Cenomanian-Turonian event. Geo Mar. Lett. 31, 525–536. https://doi.org/10.1007/s00367-011-0237-z.

Rodríguez-Tovar, F.J., Uchman, A., Martín-Algarra, A., 2009a. Oceanic anoxic event at the Cenomanian-turonian boundary interval (OAE-2): ichnological approach from the betic Cordillera, southern Spain. Lethaia 42, 407–417. https://doi.org/10.1111/j.1502-3931.2009.00159.x.

Rodríguez-Tovar, F.J., Uchman, A., Martín-Algarra, A., O'Dogherty, L., 2009b. Nutrient spatial variation during intrabasinal upwelling at the Cenomanian-Turonian oceanic anoxic event in the westernmost Tethys: an ichnological and facies approach. Sediment. Geol. 215, 83–93. https://doi.org/10.1016/j.sedgeo.2009.01.006.

Rodríguez-Tovar, F.J., Dorador, J., Martín-García, G.M., Sierro, F.J., Flores, J.A., Hodell, D.A., 2015a. Response of macrobenthic and foraminifer communities to changes in deep-sea environmental conditions from Marine Isotope Stage (MIS) 12 to 11 at the "Shackleton Site". Glob. Planet. Change 133, 176–187. https://doi.org/10.1016/j.gloplacha.2015.08.012.

Rodríguez-Tovar, F.J., Dorador, J., Grunert, P., Hodell, D., 2015b. Deep-sea trace fossil and benthic foraminiferal assemblages across glacial terminations 1, 2 and 4 at the "Shackleton Site" (IODP Expedition 339, Site U1385). Glob. Planet. Change 133, 359–370. https://doi.org/10.1016/j.gloplacha.2015.05.003.

Rogerson, M., Cacho, I., Jimenez-Espejo, F., Reguera, M.I., Sierro, F.J., Martinez-Ruiz, F., Frigola, J., Canals, M., 2008. A dynamic explanation for the origin of the western Mediterranean organic-rich layers. Geochem. Geophys. Geosyst. 9, Q07U01. https://doi.org/10.1029/2007gc001936.

Rohling, E.J., Cooke, S., 1999. Stable oxygen and carbon isotopes in foraminiferal carbonate shells. In: Sen Gupta, B.K. (Ed.), Modern Foraminifera. Kluwer, Dordrecht, pp. 239–258.

Sarhan, T., García Lafuente, J., Vargas, M., Vargas, J.M., Plaza, F., 2000. Upwelling mechanisms in the northwestern Alboran Sea. J. Mar. Syst. 23, 317–331. https://doi.org/10.1016/S0924-7963(99)00068-8.

Schiebel, R., Hemleben, C., 2017. Biogeochemistry. In: Schiebel, R., Hemleben, C. (Eds.), Planktic Foraminifers in the Modern Ocean. Springer, Berlin, Heidelberg, pp. 263–293. https://doi.org/10.1007/978-3-662-50297-6_9.

Schmiedl, G., Hemleben, C., Keller, J., Segl, M., 1998. Impact of climatic changes on the benthic foraminiferal fauna in the Ionian Sea during the last 330,000 years. Paleoceanography 13, 447–458. https://doi.org/10.1029/98PA01864.

Schmiedl, G., de Bovée, F., Buscail, R., Charrière, B., Hemleben, C., Medernach, L., Picon, P., 2000. Trophic control of benthic foraminiferal abundance and microhabitat in the bathyal Gulf of Lions, western Mediterranean Sea. Mar. Micropaleontol. 40, 167–188. https://doi.org/10.1016/S0377-8398(00)00038-4.

Schmiedl, G., Mitschele, A., Beck, S., Emeis, K.-C., Hemleben, C., Schulz, H., Sperling, M., Weldeab, S., 2003. Benthic foraminiferal record of ecosystem variability in the eastern Mediterranean Sea during times of sapropel S5 and S6 deposition. Palaeogeogr. Palaeoclimatol. Palaeoecol. 190, 139–164. https://doi.org/10.1016/S0031-0182(02)00603-X.

Schmiedl, G., Pfeilsticker, M., Hemleben, C., Mackensen, A., 2004. Environmental and biological effects on the stable isotope composition of recent deep-sea benthic foraminifera from the western Mediterranean Sea. Mar. Micropaleontol. 51, 129–152.

Schmiedl, G., Mackensen, A., 2006. Multispecies stable isotopes of benthic foraminifers reveal past changes of organic matter decomposition and deepwater oxygenation in the Arabian Sea. Paleoceanography 21, PA4213. https://doi.org/10.1029/2006PA001284.

Schmiedl, G., Kuhnt, T., Ehrmann, W., Emeis, K.-C., Hamann, Y., Kotthoff, U., Dulski, P., Pross, J., 2010. Climatic forcing of eastern Mediterranean deep-water formation and benthic ecosystems during the past 22 000 years. Quat. Sci. Rev. 29, 3006–3020. https://doi.org/10.1016/j.quascirev.2010.07.002.

Schlitzer, R., 2009. Ocean Data View. http://odv.awi.de.

Schroeder, K., García-Lafuente, J., Josey, S.A., Artale, V., Nardelli, B.B., Carrillo, A., Gacic, M., Gasparini, G.P., Herrmann, M., Lionello, P., Ludwig, W., Millot, C., Özsoy, E., Pisacane, G., Sánchez-Garrido, J.C., Sannino, G., Santoleri, R., Somot, S., Struglia, M., Stanev, E., Taupier-Letage, I., Tsimplis, M.N., Vargas-Yáñez, M., Zervakis, V., Zodiatis, G., 2012. Circulation of the Mediterranean Sea and its variability. In: Lionello, P. (Ed.), The Climate of the Mediterranean Region. Elsevier, Oxford, pp. 187–256.

Sgarrella, F., Moncharmont Zei, M., 1993. Benthic foraminifera in the Gulf of Naples (Italy): systematics and auto ecology. Boll. Soc. Paleontol. Ital. 32, 145–264.

Shackleton, N.J., 1974. Attainment of isotopic equilibrium between ocean water and the benthonic foraminifera genus *Uvigerina*: isotopic changes in the ocean during the last glacial. In: Labeyrie, J. (Ed.), Les Méthodes Quantitatives d'étude des Variations du Climat au Cours du Pléistocène. Colloques Internationaux du CNRS. CNRS Paris, Gif/Yvette, pp. 203–210.

Sierro, F.J., Hodell, D.A., Curtis, J.H., Flores, J.A., Reguera, I., Colmenero-Hidalgo, E., Bárcena, M.A., Grimalt, J.O., Cacho, I., Frigola, J., Canals, M., 2005. Impact of iceberg melting on Mediterranean thermohaline circulation during Heinrich events. Paleoceanography 20, PA2019. https://doi.org/10.1029/2004PA001051.

Stuiver, M., Reimer, P.J., 1993. Extended ^{14}C data base and revised Calib 3.0 ^{14}C age calibration program. Radiocarbon 35, 215–230. https://doi.org/10.1017/S0033822200013904.

Takahashi, T., Olafsson, J., Goddard, J.G., Chipman, D.W., Sutherland, S.C., 1993. Seasonal variation of CO_2 and nutrients in the high-latitude surface oceans: a comparative study. Glob. Biogeochem. Cycles 7, 843–878. https://doi.org/10.1029/93GB02263.

Thunnel, R., Sautter, L.R., 1992. Planktonic foraminiferal faunal and stable isotopic indicators of upwelling: results from sediment trap study in the California Current. In: Summerhayes, C.P., Prell, W.L., Emeis, K.C. (Eds.), Evolution of Upwelling Systems since the Early Miocene. Geological Society, Special Publication London, pp. 77–91. https://doi.org/10.1144/GSL.SP.1992.064.01.33.

Thunell, R., Benitez-Nelson, C., Varela, R., Astor, Y., Muller-Karger, F., 2007. Particulate organic carbon fluxes along upwelling-dominated continental margins: rates and mechanisms. Glob. Biogeochem. Cycles 21, GB1022. https://doi.org/10.1029/2006GB002793.

Toucanne, S., Jouet, G., Ducassou, E., Bassetti, M.-A., Dennielou, B., Angue Minto'o, C.M., Lahmi, M., Touyet, N., Charlier, K., Lericolais, G., Mulder, T., 2012. A 130,000-year record of levantine intermediate water flow variability in the Corsica Trough, western Mediterranean Sea. Quat. Sci. Rev. 33, 55–73. https://doi.org/10.1016/j.quascirev.2011.11.020.

Uchman, A., Wetzel, A., 2011. Deep-sea ichnology: the relationships between depositional environment and endobenthic organisms. In: Huneke, H., Mulder, T. (Eds.), Deep-Sea Sediments, Developments in Sedimentology, vol. 63. Elsevier, Amsterdam, pp. 517–556.

Westrich, J.T., Berner, R.A., 1984. The role of sedimentary organic matter in bacterial sulfate reduction: the G model tested. Limnol. Oceanogr. 29, 236–249. https://doi.org/10.4319/lo.1984.29.2.0236.

Wetzel, A., Uchman, A., 2012. Hemipelagic and pelagic basin plains. In: Knaust, D., Bromley, R.G. (Eds.), Trace Fossils as Indicators of Sedimentary Environments. Developments in Sedimentology, vol. 64. Elsevier, Amsterdam, pp. 673–701.

Wüst, G., 1961. On the vertical circulation of the Mediterranean Sea. J. Geophys. Res. 66, 3261–3271. https://doi.org/10.1029/JZ066i010p03261.